6

DARK STRUCTURES IN NONRADIATIVE PROCESSES

6.1 Introduction

Static and time-resolved spectroscopic investigations carried out with ever-increasing sophistication over the past six decades have largely shaped our current understanding of the complex interplay between radiative and nonradiative molecular processes across the chemical, physical, and biological sciences. The very nature of the light probe, however, obfuscates the detection of 'dark' *states* which have been frequently implicated but have never been *directly* observed. Utilizing ultrashort electron pulses as probes renders UED sensitive to *all structures*, and therein lies its unique potential to unravel the structural dynamics of photophysical and photochemical outcomes. This chapter showcases our UED studies of prototypical heteroaromatic molecules (pyridine and its methylated analogues) with close-lying states in the excited state manifold.

Radiationless processes abound in a wide variety of chemical, physical, and biological systems yielding a rich diversity of phenomena. For example, the nature and dynamics of the excited electronic states created in nucleic acids by UV light influences the complex chain of events that culminates in DNA photodamage with profound biological consequences, including photocarcinogenesis. After light absorption, a molecule can undergo a number of different radiationless transitions, including photochemical processes such as fragmentation, isomerization and ionization, and photophysical processes such as internal conversion between electronic states of like multiplicity and spin-orbit-coupling-dependent intersystem crossing between dissimilar spin states. For more than eight decades, our understanding of such radiationless processes has been shaped by light-based tools used to interrogate them. The absence of light emission in such nonradiative phenomena has meant that information about the states involved has only been *indirectly* inferred from their influence on the more readily observed radiative and photochemical pathways (for example, through observations of the invariance of fluorescence spectra and fluorescence yields upon exciting successive upper singlet states, and on measurements of relative yields of phosphorescence to fluorescence). Moreover, such nonadiabatic phenomena occur at or near the breakdown of the Born-Oppenheimer approximation, which has long been the cornerstone for the visualization of chemical processes. This breakdown is particularly common in complex polyatomic molecules, where there are a large number of energetically close-lying electronic states and many nuclear degrees of freedom. A particularly striking and important example of the result of the vibronic coupling between nuclei and electrons is a conical intersection between electronic states, which provide pathways for interstate crossing on ultrafast timescales.

Over the past nearly two decades, femtosecond time-resolved methods have been applied to chemical reactions ranging in complexity from bond-breaking in diatomic molecules to dynamics in supramolecular and biological molecules and have led to breakthroughs in our understanding of fundamental chemical processes. The information obtained from these experiments, however, is very much dependent on the nature of the state ‘selected’ by a given probe scheme. Spectroscopic methods involving transient absorption, nonlinear wave mixing, laser-induced fluorescence, and resonant multiphoton ionization usually require the probe laser to be resonant with an electronic transition in the species being monitored. Hence, as a chemical reaction evolves toward products, these probe methods are restricted to observation of the dynamics within a small region of the reaction coordinate. Moreover, in many studies of nonadiabatic processes in polyatomic molecules, the initially prepared ‘bright’ state is often coupled to a lower-lying ‘dark’ state. The ‘darkness’ of this resulting state greatly obscures the observation of its dynamics, and, in many cases, renders it ‘unobservable’ leading to potentially erroneous conclusions about the presence or absence of energy flow pathways.

UED, on the other hand, uses electrons as probes and is sensitive to *all* inter-atomic distances in the molecule. By removing the reliance on a resonance condition, the physics of the UED probe is fundamentally different, enabling it to follow dynamics along the entire reaction coordinate. Consequently the probe pulse need not be tunable and, more interestingly, the excited state evolution can be followed to regions far from the equilibrium configuration. Moreover, by monitoring *structure* space instead of *state* space, UED offers dramatic and unique advantages for following nonradiative processes since diffraction is always ‘allowed’ and optically dark states are as readily observed as bright ones–there are no ‘dark’ states for diffraction.

An intriguing phenomenon in the gas-phase photophysics of collision-free S_1 benzene is the observation of a dramatic decrease in the quantum yield of fluorescence for vibrational energies exceeding about 3000 cm^{-1}.[1] Correspondingly, the absorption line width of the S_0-S_1 system of gaseous benzene measured as a function of excitation excess energy reveals a sudden onset of line broadening at about this energy. These observations have led to the suggestion that, for excess vibrational energies above this threshold value, a new nonradiative relaxation process, referred to as channel three decay, comes into play. An important new observation emerging from recent experiments with jet-cooled molecules[2] is that the onset of the channel-three decay becomes even more abrupt when thermal inhomogeneous congestion is removed by supersonic expansion. An even more intriguing fact is that the nonradiative rate (k_{nr}), as measured in fluorescence lifetime experiments, is a function of the symmetry of the vibronic band excited, i.e., some types of vibrations have an enhanced k_{nr} lower in the S_1 manifold than others. This is thought to be due to the fact that some vibrations (most probably the out-of-plane vibrations) can promote nonradiative decay more effectively than others. The channel three phenomenon was discovered over three decades ago,[3] but to date no generally accepted explanation has been given. Several mechanisms have been invoked to explain the channel three process:

(1) direct radiationless transition from the lowest excited state to S_0 enhanced by intramolecular vibration (IVR)

(2) formation of an intermediate electronic state with a bound or unbound potential-energy surface, and

(3) photochemical reaction.

The mechanism invoking direct internal conversion (IC) is based on the presence of out-of-plane modes whose frequency is much lower in the lowest excited state than in the ground state. This large frequency change renders these vibrations exceptionally good accepting modes for radiationless transition between these states. In this mechanism, IVR leads to the production of excited molecules with a high degree of excitation of out-of-plane bending modes, and hence, the onset of channel three is believed to be related to the onset of IVR. The photochemical mechanism invokes the crossing of an isomeric state with the lowest excited state, whereby photochemical conversion of the S_1 molecule to an isomeric form leads to sudden opening of a new nonradiative decay channel. The third mechanism involves formation of an intermediate state, which could be an electronic state of an isomeric form or an electronic state of the parent molecule itself.

Azabenzenes are important parent molecular systems for numerous compounds such as biologically active nicotinic acid and the nucleotides cytosine, uracil, and thymine, and therefore, have been the subject of extensive experimental and theoretical studies. Azabenzenes are isoelectronic with benzene. The nitrogen atoms introduce perturbations to the benzene energy levels and give rise to new transitions due to excitation of their lone-pair electrons. Their lower electronic excitation spectra in the near and vacuum ultraviolet regions are due to both $n\pi^*$ and $\pi\pi^*$ valence transitions, and the lowest-lying transitions are of $n\pi^*$ origin; these form the basis for differences in the photophysical behavior of azabenzenes and benzene.

Pyridine, the simplest aza-aromatic molecule obtained by replacing one methine (CH) group with a nitrogen atom, has been extensively studied with regard to the photophysics and photochemistry of its low-lying excited states. Although it is often thought of as a paradigm molecule, its properties are actually somewhat unusual. Pyridine had been believed[4] to be a totally nonfluorescent molecule until 1977 when Yamazaki and Baba discovered weak fluorescence in the gas phase.[5] A subsequent study[6] revealed that the fluorescence quantum yield is only $\Phi_F = 5.9 \times 10^{-5}$ at the S_1 (n,π*) 0^0 level—two to three orders of magnitude smaller than the diazabenzenes, pyrazine (1.3×10^{-3}) and pyrimidine (1.5×10^{-2}) at their respective S_1 origins. Such a low fluorescence quantum yield implies highly efficient nonradiative processes even at the S_1 origin. Furthermore, at ~1600 cm^{-1} above the S_1 origin, pyridine undergoes an order-of-magnitude drop in the quantum yield of intersystem crossing and a 50% drop in the fluorescence quantum yield—the channel three process.

For many years, the nature of the ultrafast internal conversion in pyridine relative to those of other azabenzenes had been thought to be a solved problem. Pyridine photophysics had been interpreted in terms of the proximity effect,[7-12] which states that rapid internal conversion results from having a low-lying ππ* electronic state very near the nπ* state. Vibronic mixing between these two states leads to a large frequency change in the vibronically active out-of-plane modes in the nπ* state, which increases the Franck-Condon factors and enables these modes to serve as accepting modes in the internal conversion process. The pyridine ππ* state lies only 3500 cm^{-1} above the nπ* state, compared to a S_1–S_2, gap ranging from 7000 to 9250 cm^{-1} in the diazo molecules pyrazine, pyrimidine, and pyridazine.[13] This small energy gap was postulated to result in extensive vibronic mixing between the S_2 (ππ*) and S_1 (nπ*) states, as mediated by vibrations of A_2 symmetry. The resulting shift in the potential surface causes a large frequency change in the A_2 vibrations between the ground and electronic states, providing good Franck–Condon factors for internal conversion.

Recent experiments,[2] however, have cast serious doubt upon the assertion that efficient internal conversion in pyridine results from the proximity effect. Model calculations predict that if the proximity effect is responsible for the rapid internal conversion in pyridine, then optical excitation of out-of-plane bending modes of A_2 symmetry should effect a dramatic increase in the internal conversion rate, relative to other vibrational modes, since modes of A_2 symmetry are most efficient in vibronically coupling the S_1 and S_2 states. Recently, Villa *et al.*[2] studied the photophysics of a variety of pyridine vibronic levels in a supersonic jet. They observed that vibrational modes of A_2 symmetry are not particularly effective in promoting internal conversion, as would be expected if the proximity effect played an important role in the internal conversion process. They therefore cast doubt upon the previously generally accepted belief that efficient internal conversion in pyridine results from the proximity effect. Villa *et al.* proposed instead that rapid internal conversion may be caused by valence distortion, in which a change in the equilibrium position of the molecule upon electronic excitation results in favorable Franck–Condon factors for transitions having large changes in quantum number in the out-of-plane bending modes. This enables these modes to serve as accepting modes and enhances the internal conversion rate. However, even Villa *et al.* acknowledge that this explanation is also problematical, as a large geometry change would results in extensive vibrational activity in the displaced modes, which is not seen. There have been proposals from time to time that an excited-state photoreaction quenches the fluorescent singlet states of pyridine, but photoproducts have never been detected in the high yields necessary to explain the ultralow fluorescence quantum yields. These results suggest that we are still far away from achieving proper understanding of the photophysics of this beguiling simple molecule.

The proximity effect also enabled predictions to be made concerning the effect of substituents on the internal conversion rate.[12] Electron donating moieties are known to lower the energy of ππ* states and raise the energy of nπ* states. Thus, for chromophores whose lowest electronic transition is nπ*, adding an electron donating substituent will tend to shrink the gap between the nπ* and ππ* states. This increases the magnitude of the vibronic coupling, which in turn causes a larger change in the vibrational frequency of the vibronically active mode. The net result is an enhancement of the internal conversion rate upon substitution of an electron donating moiety. Ring substituents alter the energies of nπ* and/or πiπ* excited states of these systems, and our particular interest has been to explore the effect of these changes on the rates of nonradiative decay and the quantum yields. However, as the experiments of Baba and co-workers reveal[6, 13-15], the nonradiative decay rate actually decreases in 2-methylpyridine and completely disappears in 2,6-dimethylpyridine, in contradiction to the proximity effect.

In an effort to understand this puzzling behavior of the excited state photophysics with increasing substitution and to explore the structural manifestations of the channel three process, we performed detailed ultrafast electron diffraction (UED) studies of the structural dynamics of three azabenzenes—pyridine, 2-methylpyridine (2-picoline, α-picoline), and 2,6-dimethylpyridine (2,6-lutidine). UED, developed in our laboratory over the past 12 years and through four generations of machines, utilizes properly timed sequences of ultrafast electron pulses to image complex molecular structures in the four dimensions of space and time with resolutions of 0.01 Å and 1 ps, respectively.[16, 17] The new limits of UED provide the means for the determination of transient molecular structures, including reactive intermediates and non-equilibrium structures of complex energy landscapes. By freezing structures on the ultrafast timescale, we are able to develop concepts that correlate *structure* with *dynamics*. Examples include structure-driven radiationless processes, dynamics-driven reaction stereochemistry, pseudorotary transition-state structures, and non-equilibrium structures exhibiting negative temperature, bifurcation, or selective energy localization in bonds. Furthermore, the recent development of a new machine devoted to structures in the condensed phase, has established ultrafast crystallography as a powerful method for mapping out temporally changing molecular structures in chemistry, and potentially, in biology.[18-21]

6.2 Ground-State Structures

A. Pyridine

Figure 6–1 shows the 2D ground-state diffraction image of pyridine. The peaks in the corresponding radial distribution $f(r)$ curve (Fig. 6–2) reflect the covalent C–C and C–N distances occurring at ~1.3 Å, the second-nearest neighbor C··C and C··N distances at ~2.3 Å, and the third-nearest neighbor C···C and C···N distances at ~2.8 Å. The ground state structure has been well-characterized by gas-phase steady-state electron diffraction (GED),[22-24], X-ray crystallography,[25] microwave spectroscopy,[26] infrared spectroscopy,[27-29] overtone spectroscopy,[30] and various computational methods[30-35]. Figure 6–3 shows the least-squares refined structure of the pyridine ground state. The parameters are in excellent agreement with previous experimental structures as well as recent high-quality quantum chemical calculations. While the earliest GED investigations of pyridine by Schomaker and Pauling[22] and Almenningen *et al.*[23] were not able to address this change in the CNC angle owing to the limited possibilities of their time, the more recent GED results of Pyckhout *et al.*[24] did reveal this effect. Their GED structure also indicated that the ortho, meta, and para C–H bonds in pyridine are nonequivalent and that the meta CH bond is shorter than the para CH bond, which in turn, is shorter than the ortho CH bond; this has been confirmed by recent CH stretching overtone spectra[30] in conjunction with various *ab initio* calculations. However, given the orders-of-magnitude lower electron beam current of pulsed UED vis-à-vis static GED[17] and the relative insensitivity of electron diffraction to hydrogens, our ground state results do not capture this relative ordering of the C–H bond lengths.

B. 2-Picoline

Figure 6–4 shows the 2D ground-state diffraction image of picoline. The peaks in the corresponding radial distribution *f*(*r*) curve (Fig. 6–4) reflect the covalent C–C and C–N distances occurring at ~1.3 Å, the second-nearest neighbor C··C and C··N distances at ~2.3 Å, and the third-nearest neighbor C···C and C···N distances at ~2.8 Å. While all the peaks have similar mean positions as pyridine, note that the addition of the methyl group introduces several long indirect C···C distances that result in a broadening of the peak at ~3.7 Å. While the ground state structure of picoline has been previously determined by X-crystallography at 120 K[36] and 153 K,[37] our study is the first determination of the isolated picoline molecular structure by electron diffraction. Figure 6–5 shows the best-fit structural parameters of the picoline ground state. Again, the aromatic ring distances are nearly unchanged from pyridine and picoline.

C. 2,6-Lutidine

Figure 6–6 shows the 2D ground-state diffraction image of lutidine and Fig. 6–7 shows the 1D radial distribution curves in comparison with the other azines. The peaks in the radial distribution *f*(*r*) curve reflect the covalent C–C and C–N distances occurring at ~1.3 Å, the second-nearest neighbor C··C and C··N distances at ~2.3 Å, and the third-nearest neighbor C···C and C···N distances at ~2.8 Å. While all the peaks have similar mean positions as pyridine and picoline, note that the addition of the second methyl group introduces longer indirect C···C distances which results in further broadening of the peak at ~4.0 Å (see Fig. 6–7). No previous electron diffraction study has been performed on 2,6-lutidine, although the crystal structure at 120 K has been determined.[38] Using molecular orbital calculations at the SCF level, Porcinai and Foggi[39] report that the most stable rotamer of 2,6-lutidine has C_{2v} symmetry with one of the C–H bonds of both methyl groups lying in the plane of the ring and pointing in the opposite direction with respect to the nitrogen atom. Figure 6–8 presents the refined ground-state parameters of lutidine obtained by UED.

6.3 Transient Structures

A. Pyridine

To resolve the structural changes during the course of the reaction, we collected UED images for a range of time delays from –90 ps to +185 ps. The 2D diffraction-difference images (with the image at –90 ps chosen as the reference image) clearly exhibit the emergence of periodic ring patterns (Fig. 6–9), whose intensity becomes more pronounced over time. These rings in the diffraction-difference images directly reflect the changes in the molecular structure from the reference structure at –90 ps. The corresponding 1D difference curves, $\Delta f(t;\ t_{\text{ref}};\ r)$, shown in Fig. 6–10 exhibit peaks with both negative and positive amplitudes: *the negative peaks (shaded blue) represent the depletion of covalent* (~1.3 Å region) *and second-nearest neighbor* (~2.5 Å region) *distances, whereas positive peaks* (shaded red) *denote the formation of new internuclear pairs* (those, with distances of ~ 1.1 and 1.3 Å and those with distances greater than 3.5 Å).

Upon excitation, several possible reaction pathways are open to the pyridine molecule, including valence isomerization, fragmentation, and ring opening, as indicated in Scheme 6–1. Figure 6–11 depicts some structures proposed in the literature for the photochemistry of pyridine: gas phase (Dewar- and Hückel-type isomers[40] and C_4H_4 + HCN fragmentation[40, 41]); liquid phase (Dewar isomer,[42] azaprefulvene isomer[43]); matrices (Dewar isomer[44-46] and C_4H_4 + HCN fragmentation[44, 46]), and quantum-chemical calculations (azaprefulvene isomer[43, 47]). To discriminate between the various possible reaction channels, the UED data was fit to a series of structural models. Figure 6–12 shows the comparison between the experimental transient-isolated $f(r)$ curves averaged over four time slices (from +60 ps to +185 ps) and the corresponding theoretical curves for various trial structures (adjusted for excess internal energy). The poor agreement between theory and experiment for the vibrationally hot Kekulé, Dewar, Hückel, azaprefulvene, and C_4H_4 + HCN fragmentation channels precludes these structures from being involved in the dominant reaction channel on our time scale. When a mixture of Dewar, Hückel, and vibrationally 'cold' (403 K) ring-opened diradical structures was fit to the experimental $f(r)$ curve, this multi-component fit indicated that ring opening was the major channel, with the isomerization to the Dewar structure being the minor one; the contribution of the Hückel isomer was vanishingly small.

A superior structural fit was obtained using just the ring-opened structure albeit with increased internal energy, manifested by mean amplitudes of vibration 70–100% higher than those of the cold structure at 403 K. These higher vibrational amplitudes—reflected as damping and peak broadening in the experimental $f(r)$ curves—could easily result from a non-thermal (non-Boltzmann) population in the molecule's vibrational degrees of freedom, as has been elucidated by UED in pericyclic reactions.[48] In the presence of such hot ring-opened structures, the relative fractions of the Dewar and Hückel structures become negligible in a multi-component fit. These results establish that the primary product is a hot ring-opened diradical structure.

Figure 6–13 shows the ring-opened structure following least-squares refinement of vibrational amplitudes and internuclear distances, with the corresponding $sM(s)$ and $f(r)$ curves being shown in Fig. 6–14. The features of this refined structure are consistent with the diffraction-difference curves of

Fig. 6–10; for instance, C(1)–N distance of ~5.23 Å and C(1)–C(5) distance of ~4.33 Å correspond to the emergence of long internuclear separations, and hence, the loss of covalent and next-nearest neighbor distances. As shown in Fig. 6–13, the best-fit covalent-bond distances and all but one of the angles are consistent with quantum-chemical calculations performed in this laboratory. The primary exception is one of the skeletal torsional angles, which, with a best-fit value of ~123° (instead of 180°), distorts the planarity of the predicted ring-opened structure and places the N-atom ~60° above the plane defined by the C-skeleton. Because UED measures the structure obtained for all molecules, this result must reflect the multiple torsional conformations, in concordance with a flexible structure. Also, as can be seen from the final refined structures of the ground state and the transient intermediate in Figs. 6–3 and 6–13, the skeletal carbon–carbon bond distances change from being aromatic in the ground state (~1.4 Å) to become aliphatic in the diradical (C–C ~ 1.46 Å and C=C ~ 1.35 Å).

We obtained the structural evolution of the transient-isolated $f(r)$ curves, as shown in Fig. 6–15. Except for their relative intensities, the shapes of the transient-isolated curves were nearly indistinguishable over time—indicating that the transient structure remains nearly unchanged on the time scale of the experiment; its population alone changes. A least-squares fit of the transient population gave a time constant of 17 ± 1 ps (Fig. 6–16). These results, in conjunction with the difference curves in Fig. 6–10, indicate that, upon excitation, the ultrafast ring opening of pyridine disrupts its aromaticity, and the ensuing open structure increases in population with a time constant of ~17 ps.

B. 2-Picoline

Upon excitation, several possible reaction pathways are open to the picoline molecule, including valence isomerization, fragmentation, and ring opening. To discriminate between the various possible reaction channels, the UED data was fit to a series of structural models, some of which are shown in Fig. 6–17. A superior structural fit was obtained using the ring-opened structure establishing that the primary product is a hot ring-opened diradical structure.

Figure 6–18 shows the ring-opened structure following least-squares refinement of vibrational amplitudes and internuclear distances, along with the corresponding $sM(s)$ and $f(r)$ curves. The best-fit covalent-bond distances and all but one of the angles are consistent with quantum-chemical calculations performed in this laboratory. We obtained the structural evolution of the product, as shown in Fig. 6–19. A least-squares fit of the transient population gave a time constant of 28.7 ± 7 ps.

C. 2,6-Lutidine

The 1D difference curves, $\Delta f(t;\, t_{\mathrm{ref}};\, r)$, shown in Fig. 6–20 exhibit peaks with both negative and positive amplitudes. Upon excitation, several possible reaction pathways are open to the lutidine molecule, including valence isomerization, fragmentation, and ring opening. To discriminate between the various possible reaction channels, the UED data was fit to a series of structural models some of which are shown in Fig. 6–21.

Figure 6–22 shows the comparison between the experimental transient-isolated $f(r)$ curves and the corresponding theoretical curves for various trial structures (adjusted for excess internal energy). The good agreement between theory and experiment for the vibrationally hot ground state structures establishes internal conversion to the ground state as the dominant channel. As can be seen from Fig. 6–22, the ring opening channel gives a much poorer fit. A least-squares fit of the transient population gave a time constant of 16.1 ± 2.3 ps, as shown in Figs. 6–23 and 6–24.

6.4 Photochemistry

A. Pyridine

The photochemical behaviour of pyridine has been the subject of numerous studies that reveal a rich array of reactions and invoke different intermediates as a function of the excitation wavelength and the phase.

Moreover, many different (and often contradictory) mechanisms have been proposed for the observed behavior. 254 nm irradiation of pyridine in the liquid phase was found to proceed via photoisomerization to a Dewar pyridine (2-azabicyclo[2.2.0]hexa-2,5-diene), which rearomatized completely to pyridine within 15 min at room temperature.[42] On the other hand, at the same wavelength, Caplain *et al.*[49] suggested the presence of an azaprismane intermediate to explain their observed substitution products of pyridine.

In low-temperature rare-gas matrices, Chapman *et al.*[44] reported the formation of hydrogen cyanide and cyclobutadiene upon photolysis of pyridine at lower energies (> 290 nm) and speculated about Dewar pyridine as a possible intermediate, although no evidence was presented to support this. In contrast, the analysis of infrared product bands by Johnstone *et al.*[45] revealed no fragmentation products, but rather a photoproduct that was somewhat arbitrarily assigned to Dewar pyridine in analogy with liquid pyridine,[42] although the possibility of other isomers was not ruled out. A recent matrix-isolation infrared spectroscopic experiment[46,50] reported that the fragmentation products (HCN and C_4H_4) are produced by two channels: (i) direct photodissociation of pyridine (major channel), and (ii) secondary dissociation of Dewar pyridine (minor channel).

Early studies of pyridine photolysis in static gas led to the conclusion that pyridine vapor is unreactive[51] when excited to the S_1 (n, π*)[52] or the S_2

(π, π*)[52, 53] states. At shorter wavelengths, Mathias and Heicklen[54] reported that acetylene is the main product albeit with low quantum yields; however, they acknowledge that their results were limited by an inability to detect certain product fragments (i.e., HCN) due to reactions occurring on the chromatographic column. Lee and co-workers[41, 55] combined molecular beams with photofragment translational spectroscopy to determine the primary products formed in unimolecular photodissociation of pyridine. At 193 nm,[41] pyridine photodissociates to give HCN + C_4H_4 (59%), CH_3 + C_4H_2N (21%), C_3H_3 + C_2H_2N (11%), and H + C_5H_4N (9%) while at 248 nm,[55] the relative contributions are 80%, 1%, 0%, and 5%, respectively. However, more recent deuterium scrambling studies[56] have shown that pyridine undergoes photoisomerization to give transposition products via an azaprefulvene (and not Dewar) intermediate upon $S_0 \rightarrow S_2$ (π, π*) excitation at 254 nm in the vapor phase.

Over the past few years, we have investigated pyridine photochemistry on the ultrafast time scale using femtosecond time-resolved mass spectrometry in the gas phase[40] and femtosecond transient absorption spectroscopy in the liquid phase.[43] In the gas phase, upon 277 nm excitation, we observed a fast decay component of 400 fs (which reflects the initial displacement of the wavepacket and IVR in the reactive channel) and two slower time constants of 3.5 ps and 15 ps, which were assigned to isomerizations to Dewar and Huckel pyridines, respectively, based purely upon the energetics. However, upon two-photon excitation at 307 nm, the dynamics is drastically different, resulting in the formation of ring opened pyridine in ~80 fs which then decays in ~130 fs to form the final products, HCN + C_4H_4. The liquid phase experiments show the two distinct timescales, with the fast decay (~2.2 ps) resulting from the reactive deactivation of the S_2 (π, π*) state via isomerization to azaprefulvene, and the slow decay (~9–23 ps, depending on the solvent) resulting from the nonreactive deactivation of the S_1 (n, π*) state, mostly by intersystem crossing to the triplet. Using *ab initio* methods we found a conical intersection between the PES of S_2 (π, π*) and S_0 states responsible for the ultrafast deactivation of the pyridine molecule; the S_2 (π, π*) excited state correlates to the ground state of azaprefulvenic pyridine.

In order to elucidate the exact nature of the ring opening process, we consider two possible reaction pathways on the excited state surface following excitation into the higher vibrational levels of S_1: (i) loss of the α-H atom to form the o-pyridyl radical, followed by ring cleavage to give the open radical, and (ii) direct C–N bond scission to give the ring opened diradical. While each of these processes can also occur in the vibrationally hot molecule on the electronic ground state following $S_1 \rightarrow S_0$ internal conversion, we do not observe the hot parent structure despite the proven sensitivity of our UED apparatus to hot molecules,[48] thus precluding the participation of the hot ground state in the reaction pathway.

The observation that ring opening occurs in 2-methylpyridine and does not occur in 2,6-dimethylpyridine (see below) might lead one to believe that the presence of α-H atoms plays a critical role in the ring opening process—thereby giving more credence to the H loss initiated channel. Thermal decomposition of pyridine in shock tube pyrolysis experiments has been interpreted by Mackie *et al.*[57] as a chain reaction initiated by C–H bond scission. Although C–H bond scission in pyridine can lead to three unique pyridyl radicals, Mackie's well-accepted mechanism of pyridine pyrolysis favors the o-pyridyl radical because of its ability to produce an open-chain cyano radical directly, which is expected to be overwhelmingly more stable than any other open-chain radicals produced by the ring fissure of pyridyl radicals. Subsequent theoretical calculations[58-61] have confirmed C–H bond scission in pyridine preferentially produces the o-pyridyl radical because the C–H bond ortho to the nitrogen is weaker by ~5 kcal/mol than the other two C–H bonds. The reduced strength of the C–H bond next to the nitrogen atom (~105 kcal/mol) relative to the parent benzene molecule (~112 kcal/mol)[62] has been attributed to the stabilization effected by the interaction of the nitrogen lone pair with the adjacent C atom radical site. Calculations[61, 63, 64] also indicate that ring-opening via C–N bond cleavage in o-pyridyl radical is more favorable than C–C bond cleavage, as the former has a significantly lower activation barrier, and the resulting open-chain cyano radical C_4H_3CN is more stable than other linear C_5NH_4 radicals. However, the transient ring opened structure as revealed by UED does not arise from a C–H loss mechanism for the following reasons:

(1) The energy required to produce the o-pyridyl radical from pyridine is ~105 kcal/mol and the barrier for the o-pyridyl ring scission to produce the open chain radical is ~40 kcal/mol,[61] implying a total energy requirement of ~145 kcal/mol. However, at 403 K with a photon energy of 107 kcal/mol, there is not enough energy to cleave the ring in our experiment via this pathway.

(2) Photodissociation of pyridine and benzene reveals notable differences between the two molecules in their photochemical pathways. In the photodissociation of benzene, 96% of the dissociation events result in the loss of one or two hydrogen atoms.[65] Pyridine, in contrast, loses a hydrogen in only 9% of events; the remaining percentage consists of events that result in the destruction of the ring structure.[41, 55] This absence of the H loss channel in the unimolecular dissociation of pyridine precludes the formation of pyridyl radicals.

The ring opened diradical structure, therefore, results from direct C–N bond scission on the excited state surface. The near absence of pyridyl radicals (H atom loss) in the 193-nm photolysis of pyridine vis-à-vis the dominance of the benzyl radical (H atom loss) in benzene photodissociation convincingly demonstrates that the presence of the nitrogen in the aromatic ring opens up other reactive pathways with lower activation energy. A direct measure of the weakening of the C–N bond in pyridine *vs.* the C–C in benzene is represented by the predicted bond orders of these bonds. In benzene, all of the C–C bonds are equivalent with 66.7% double bond character, whereas in pyridine, the C–N bond order is smaller[32], resulting in C–N bond cleavage being more facile in pyridine than the analogous C–C bond rupture in benzene. C–N bond breakage in pyridine requires ~70 kcal/mol; in contrast, C–C bond breakage requires ~85 kcal/mol.[40] The relative ease of the C–N bond breakage in pyridine leads to the dominance of the HCN + C_4H_4 products (59%) at 193 nm, which can arise from further reaction of the open chain diradical. Similar stepwise elimination of HCN through a diradical intermediate has been invoked to explain the unimolecular photodissociation of pyrazine.[55, 66] Thus, both experimental observations—the near-absence of the pyridyl channel and the dominance of the HCN channel—can be explained by the ring opened diradical intermediate. Previous DFT calculations[40] estimate that the ring opening of pyridine requires ~40 kcal/mol to overcome the resonance energy and ~70 kcal/mol to break one C–N bond. Since the estimated resonance energies for pyridine vary from ~18 kcal/mol[32, 67] to ~26 kcal/mol,[32, 68] the ring-opening energy (~110 kcal/mol) calculated by Zhong *et al.*[40] is most likely overestimated. Moreover, based on the correlation of the channel-three onset to the barrier of the ring opening process (discussed below), we estimate the empirical ring-opening energy to be ca. 102–104 kcal/mol. Since the subsequent reaction to HCN + C_4H_4 requires an additional ~30 kcal/mol,[40] the molecule at 266 nm remains trapped as an open chain diradical on the time scale of our experiment (Fig. 6–16). This can also explain the apparent lack of reactivity of pyridine vapor at 254 nm reported by earlier investigators—at this energy (~113 kcal/mol), the diradical arising out of ring opening would be unable to react further to give the fragmentation products and would most likely undergo recyclization to reform the parent structure at longer times.

Based upon the above discussion, the following picture emerges for the unimolecular photodissociation of pyridine. Initial excitation with the 266 nm femtosecond light pulse prepares the pyridine molecule in the $S_1(n, \pi^*)$ state with ~2700 cm^{-1} (8 kcal/mol) excess vibrational energy. The molecule then predominantly undergoes direct C–N bond scission on the excited state surface to form the ring open diradical with a time constant of ~17 ps. There is also a minor channel which involves isomerization to Dewar pyridine. With this direct structural information of the transient intermediate elucidated by

UED, we can now revisit our earlier femtosecond mass spectrometric results.[40] The ~3.5 ps timescale can still be assigned to the Dewar isomer (which is a minor channel in the time-resolved mass spectra as well as in our UED data). However, the ~15 ps time scale (earlier ascribed by mass spectrometry to Hückel isomerization based on purely energetic considerations) is remarkably similar to the 17 ± 1 ps timescale of the UED ring opening process. Furthermore, the reported insensitivity of the timescales to deuteration (~15 ps for pyridine-h_5 *vs.* ~16 ps for pyridine-d_5) would be very surprising for the Hückel pathway given that valence isomerization involves the motions of two deuterium atoms. On the other hand, the direct ring opening process would not be sensitive to deuteration and could easily explain the lack of change in the timescales. Based on these considerations, therefore, we reassign the ~15 ps decay rate from the mass spectrometric experiment to the pyridine ring cleavage process.

B. 2-Picoline

In contrast to pyridine, there have been few photochemical studies of picoline reactivity. Caplain and Lablache-Combier[69]reported that 2-picoline, when irradiated in the gas phase at 254 nm, undergoes photoisomerization to yield 4-picoline. This is in contrast to the report by Roebke[70] that the gas-phase photolysis of 2-picoline at 248 nm yields both 3- and 4-picoline in a ratio 10:1, while photolysis at 266 nm yields 4-picoline alone with a quantum yield of 9 x 10^{-5}. To account for these photoisomerizations, both reports suggested a ring transposition mechanism involving azaprismane intermediates. Roebke also reports that irradiation of liquid picoline at 248 nm and 265 nm did not produce any products. Dewar 2-picoline with the C3–C6 bridging bond was observed in low-temperature argon matrices upon UV irradiation at 254 nm.[50, 71]

That 2-picoline undergoes ring opening to produce the diradical with a time constant of 26.7 ± 6.7 ps is clear from the analysis discussed above. Because of the methyl group in α position to the nitrogen atom, C–N bond breakage in 2-methylpyridine can take place in two ways: between the nitrogen atom and the carbon atom of the methine group, or between the nitrogen atom and the carbon atom carrying the methyl group. The structural refinement of the transient intermediate shows that 2-methylpyridine ring opens preferentially on the side that does not contain the methyl group. It is interesting to note here that studies[72] on the role of β hydrogen atoms of the methyl group in the hydrodenitrogenation of 2-methylpyridine show that the ring opening of 2-methylpiperidine occurred preferentially between the nitrogen atom and the methine group, rather than between the nitrogen atom and the carbon atom bearing the methyl group, owing to the methyl group constituting a strong steric hindrance for the right adsorption conformation of the nitrogen atom and the β H atoms.

As in pyridine, 2-picoline can undergo ring opening in one of two ways: (i) loss of the β-H atom from the methyl group to form the 2-picolyl radical, followed by ring cleavage to give the open radical,[73] which can further fragment into HCN + C_4H_4; and (ii) direct C–N bond scission to give the ring opened diradical. While each of these processes can also occur in the vibrationally hot molecule on the electronic ground state following $S_1 \rightarrow S_0$ internal conversion, the poor fits of the hot parent structure render this pathway unacceptable. Again, as was the case in pyridine, the picolyl radical channel is unfeasible due to energetic considerations as this channel requires ~140 kcal/mol to open the ring.[73] Hence, the picture that emerges is similar to pyridine in that direct C–N bond scission occurs on the excited state. The preferential scission of the bond between the nitrogen atom and the methine group can be understood in terms of the atomic charge distribution in the S_1 state as calculated by Kudoh *et al.*[71] at the CIS/6-31++G** level. Their results reveal that while the charges on N_1, C_3, C_4, and C_6 are negative, those on C_2 and C_5 are positive—implying that the N_1–C_2 and C_4–C_5 bonds have double bond character while N_1–C_6 bond has single bond character, which is easier to cleave.

C. 2,6-Lutidine

Caplain and Lablache-Combier[69] reported that 2,6-lutidine, when irradiated in the gas phase at 254 nm, undergoes photoisomerization to yield 2,4-lutidine exclusively, which they postulate occurs via azaprismane intermediates that could arise from Dewar isomers. However, as pointed out by Pavlik *et al.*,[74] this mechanism imposes arbitrary selectivity upon the possible modes of formation of the initially formed Dewar pyridines as well as on the rearomatization of the subsequently formed azaprismanes. Recent experiments present contrasting results in that vapor-phase photolysis of 2,6-lutidine at 254 nm yields 2,3-lutidine (15%), 3,4-lutidine (4%), 2-picoline (1%), trimethylpyridine (14%), and polymer (66%) whose ^{1}H NMR analysis showed the presence of aliphatic hydrogen but no absorptions due to aromatic protons, suggesting that polymerization is accompanied by ring opening. Based on the major phototransposition products and various photochemical crossover experiments, they suggest that the isomerization of 2,6-lutidine occurs via 2,6-bonding to the azaprefulvene diradical, followed by nitrogen migraton and rearomatization. These observations were later rationalized by a theoretical characterization of the photoisomerization channels on the singlet and triplet potential energy surfaces[31] by suggesting that in addition to the azaprefulvene intermediate, the azabenzvalene intermediate could also account for the singlet phototransposition products.

Our UED data suggests that upon S_2 excitation at 266 nm, 2,6-lutidine undergoes internal conversion to the ground state producing vibrationally hot 2,6-luidine along with its isomers with a time constant of 16.1 ± 2.3 ps. With the 3 ps time resolution of the UED technique, we have not observed either the azaprefulvene or azaenzvalene intermediates as discussed above. The lack of ring opening in 2,6-lutidine can be attributed to the fact that unlike pyridine and picoline, which are excited to high vibrational levels in S_1, lutidine is excited to S_2, and hence, can undergo very different reaction pathways. Moreover, as shown by the *ab initio* calculations of π Mulliken population data,[39] the presence of the two methyl groups in 2 and 6 positions stabilizes the pyridine ring as a consequence of an increased charged density: a nitrogen atom can better accommodate a higher π density.

6.5 Photophysics

The direct observation of the S_1 decay rate was performed by Yamazaki and co-workers for a number of S_1 levels of pyridine vapor in 1982, and its lifetime was 42 ps at the S_1 0^0 level. The lifetime of S_1 in solution is in the range of 9–23 ps, depending on the solvent.[43] Ultrafast electronic dephasing from the $S_1(n\pi^*)$ state was studied by time-resolved photoelectron imaging[75] in conjunction with (1+2′) resonance-enhanced multiphoton ionization (REMPI) via the S_1 state. The lifetime at the S_1 origin was determined to be 32±5 ps from the decay of the total photoionization signal.

The above UED observations for pyridine are directly relevant to the 'channel three' non-radiative process. In our UED experiment on pyridine, the excess vibrational energy in $S_1(n, \pi^*)$ is ~2,700 cm^{-1}—well above the ~1,600 cm^{-1} threshold for 'channel three' behavior in pyridine. For picoline, the 266 nm photon prepares the molecule with ~2742 cm^{-1} excess energy in the $S_1(n, \pi^*)$ state—also above the picoline 'channel three' threshold. In lutidine, however, the pump pulse lands the molecule on the $S_2(\pi, \pi^*)$ with ~595 cm^{-1} excess energy in the second excited electronic state.

Historically, various explanations have been invoked to account for the channel three behavior; however, our UED data for pyridine and picoline does not support the following proposed scenarios: (i) direct $S_1 \rightarrow S_0$ internal conversion, which would land the molecule on the electronic ground-state with a concomitant increase in internal energy, making it vibrationally hot. We do not observe the hot parent structure despite the proven sensitivity of our UED apparatus to hot molecules; (ii) isomerization-mediated internal conversion (e.g., via the Dewar, Hückel, or azaprefulvene structures), which can also be ruled out based on the poor fits to these isomers (Fig. 6–12).

For aromatic pyridine and picoline, the nonradiative channel-three behavior is due to direct ring opening to form the diradical structure obtained above. This is in stark contrast to the prevailing view that an ultrafast internal conversion pathway, mediated by the proximity of the first and second excited state surfaces, opens up at the channel three threshold leading to vibrationally-hot ground-state molecules. However, lutidine does not undergo ring opening, accounting for the lack of channel three behavior. This structural change explains the behavior in quantum yield observed in this series of molecules—in the channel three region pyridine and picoline show a change with vibrational energy (35,000–40,000 cm^{-1}) while lutidine does not, even though for all the initial (0,0) decay is similar and the yield is low in value due to the proximity of states. The ring opening pathway can also clarify other observations made in different phases, as will be detailed elsewhere.

The observed disparity in the transient intermediates for this homologous series of azabenzenes begs the question—why are profound differences in photophysical and photochemical behavior induced by subtle changes in the parent molecular structure? In pyridine, optical excitation at 266 nm involves the removal of a non-bonding electron on the nitrogen atom to the antibonding π^* orbital of the ring, thus lowering the strength of the C–N bond and resulting in its facile scission. If the time scale of this bond rupture is shorter than the lifetime of the state at that particular total energy, we expect this highly efficient nonradiative photochemical process to actively deplete the radiative population, causing a decrease in emission quantum yield. The abruptness of the onset of the channel-three phenomenon is, therefore, a manifestation of the energy threshold for the ring-cleavage chemistry.

Upon methyl substitution, the electron-donating nature of these groups increases the electron density on the ring, leading to greater stability. Despite this increase in ring strength, structural refinement shows that 2-methylpyridine does indeed open the ring, preferentially on the side that does not contain the methyl group. This favored scission of the bond between the nitrogen atom and the methine group can be understood in terms of its weaker character relative to other skeletal bonds in the S_1 state. On the other hand, the presence of two methyl groups in 2- and 6- positions of lutidine further stabilizes the ring as a consequence of an increased charged density, and it is not surprising that the nonradiative process is photophysical internal conversion and not photochemical ring opening. The quantum yield measurement reflects this behavior of electronic structure changes (not density of vibrational states argument) as 3-picolne reverts to a pyridine-type behavior. It should be noted that addition of electron-donating methyl substituents tends to shrink the gap between the close-lying first (nπ*) and second (ππ*) excited states, and this effect is important for the overall decay even with no excess vibrational energy.

There is also a remarkable similarity in the measured and estimated decay rates of the singlet states with the time constants determined by UED. The S_1 decay rate of pyridine at the channel three threshold measured to be 20 ps is remarkably similar to the product growth rate of ~ 17 ps of the open diradical, further supporting the direct nature of the C–N bond scission on the excited hypersurface.

6.6 Conclusions

UED has probed the paradigm case of bond breaking and bond making in the prototypical nitrogen heterocycle, pyridine, and its methylated analogues. As detailed above, UED has been successful not only in identifying the dominant reaction channel among this plethora of possibilities, but also in elucidating the transient structure of the reaction intermediate. UED, for the first time, uncovered a previously unknown ring-opened diradical intermediate structure resulting from C–N bond scission in pyridine and picoline (Fig. 6–25)—this observed ring-opened structure casts new light on the decades-old puzzle of channel-three behavior occurring in many aromatic molecules. The ring-opened diradical structure was isolated from among a plethora of possibilities for reaction pathways. Through determination of the reactant and transient molecular structures, we are able to relate the structural changes in bond distances and angles to the timescale of population changes involved in bond breaking and bond making. The direct correlation of the photochemical and photophysical timescales underscores the ability of ultrafast electron diffraction to elucidate ultrashort structural dynamics of isolated molecules subjected to complex radiative and nonradiative pathways.

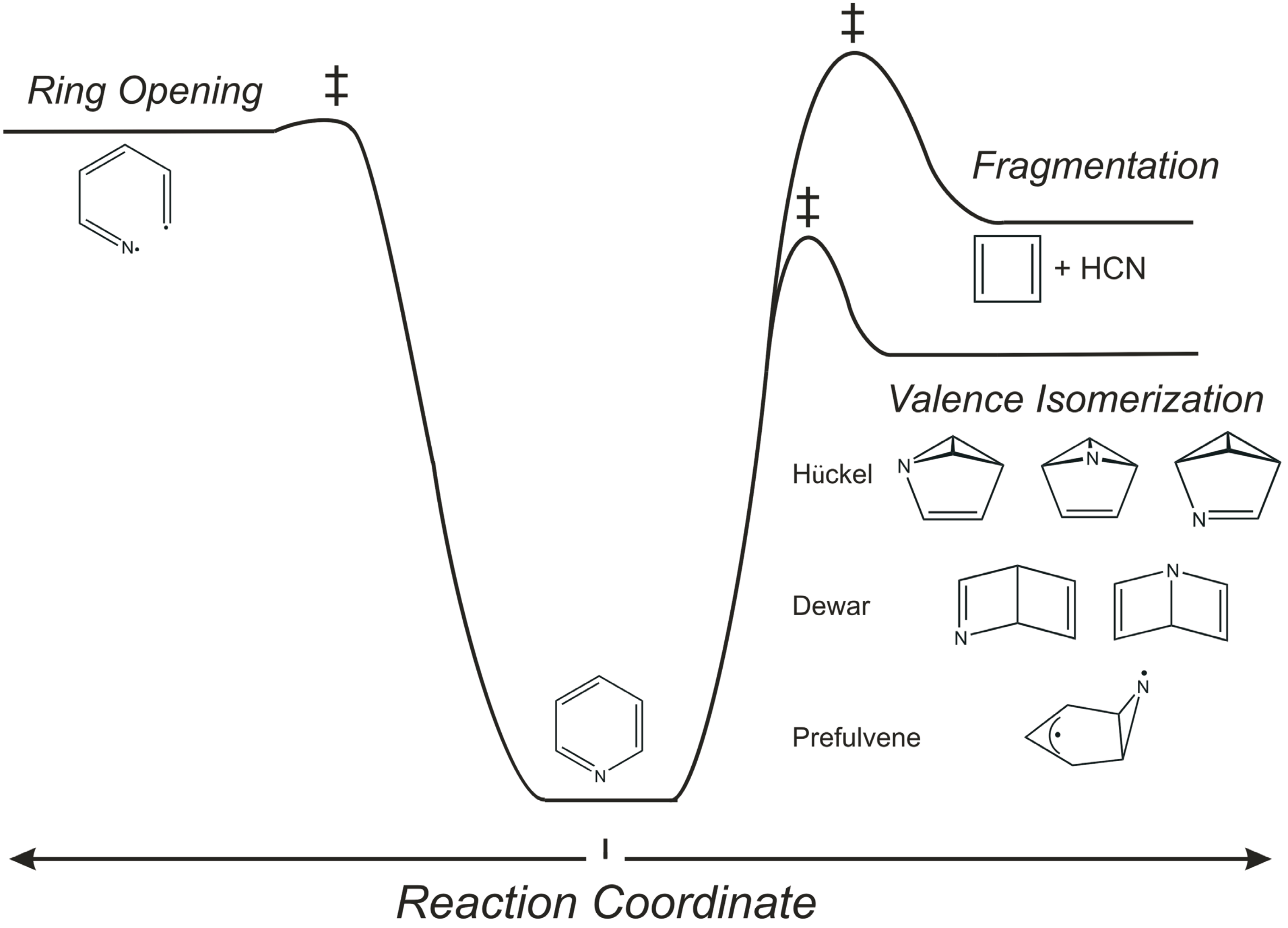

Scheme 6-1. Pyridine reaction with multiple reaction pathways.

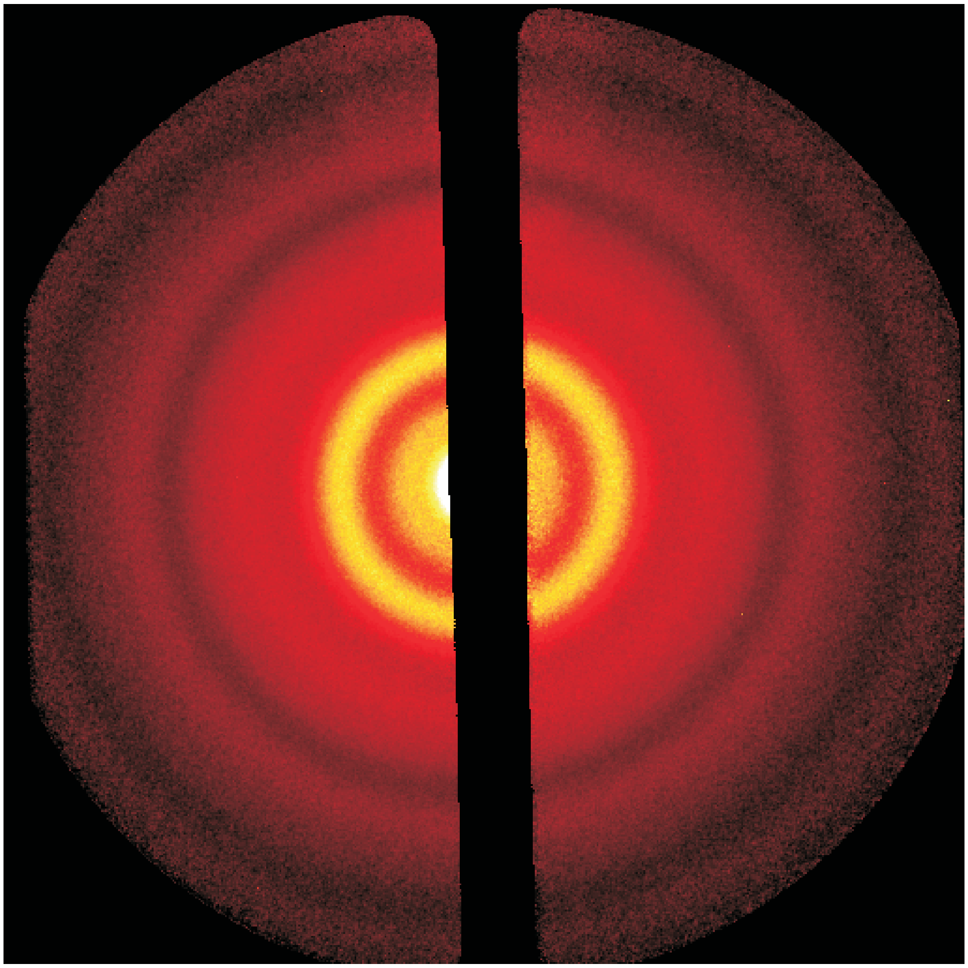

Figure 6-1. Ground-state molecular diffraction image of pyridine.

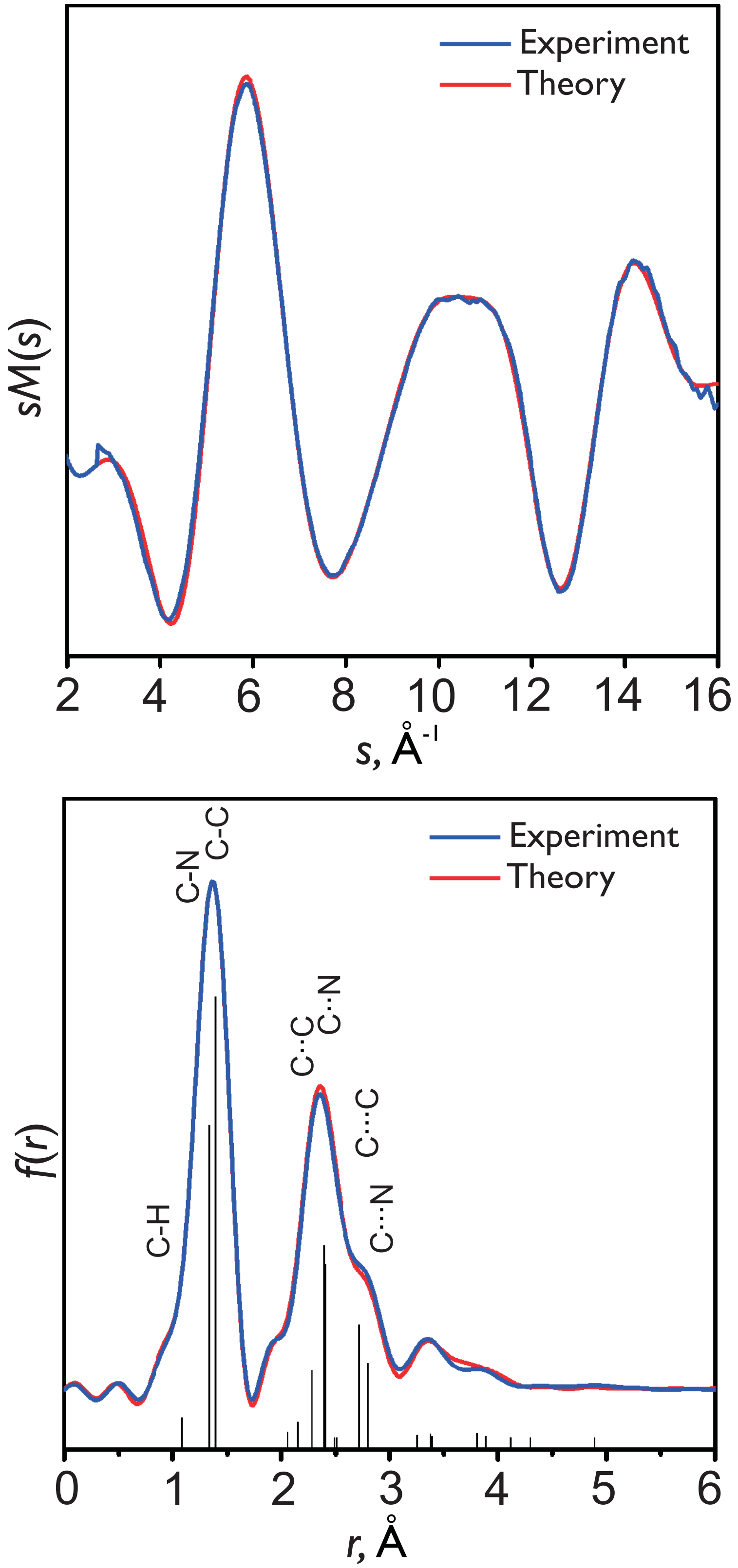

Figure 6-2. Refined ground-state structure of pyridine. Comparison between the experimental and refined theoretical *sM*(*s*) and *f*(*r*) curves is shown.

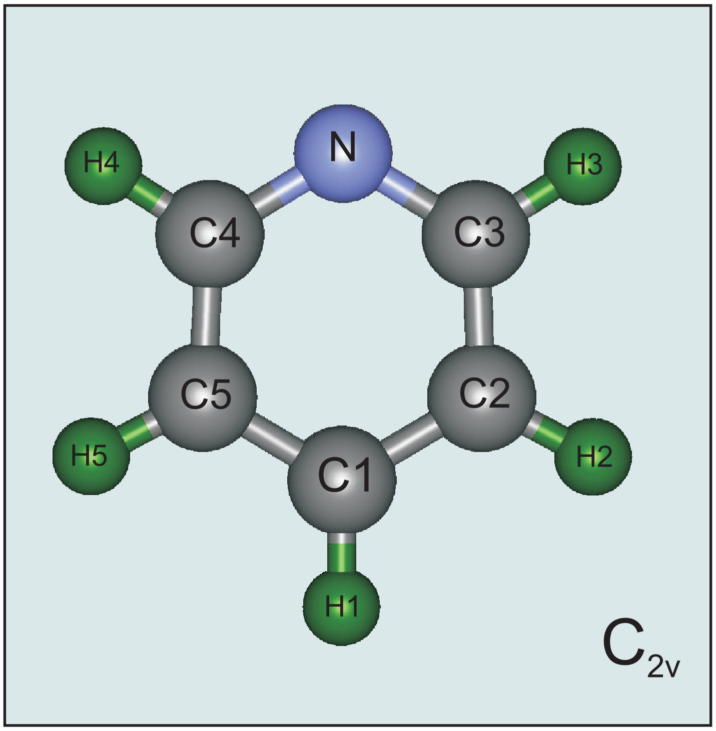

Distances

	experiment	*DFT*
r (C1-C2)	1.420 ± 0.002	1.391
r (C2-C3)	1.414 ± 0.004	1.394
r (C3-N)	1.308 ± 0.07	1.336
r (C1-H1)	1.100 ± 0.005	1.084
r (C2-H2)	1.112 ± 0.007	1.083
r (C3-H3)	1.089 ± 0.005	1.086
r (C1-N)	2.803 ± 0.009	2.80

Angles

α(H1-C1-C2)	121.6 ± 0.58	120.7
α(C1-C2-C3)	118.6 ± 1.02	118.5

Figure 6-3. Refined ground-state structure of pyridine. Distances are in ångströms and angles are in degrees. The C3–N distance was not independently refined, but derived from other best-fit (refined) distances in the structure.

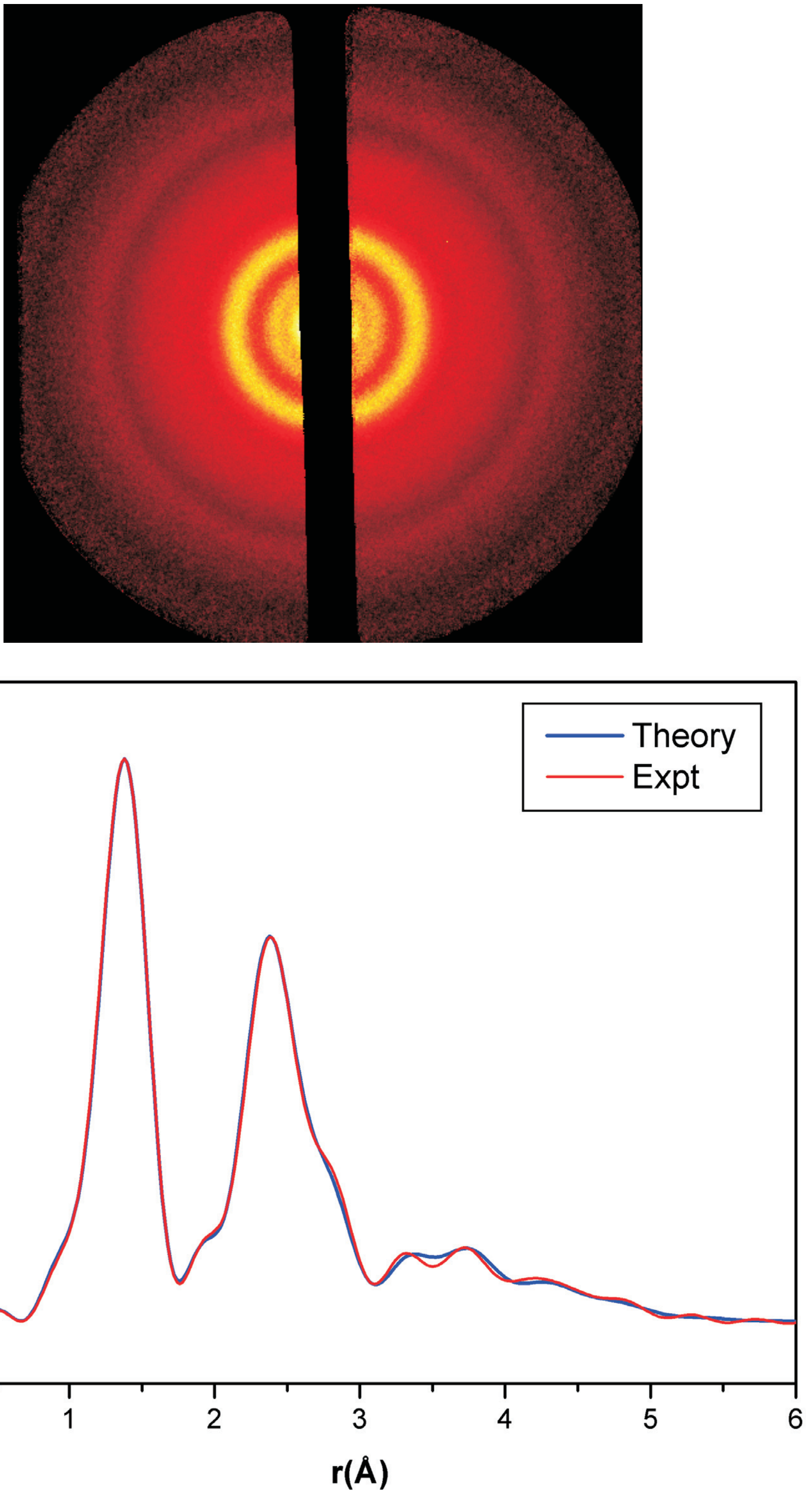

Figure 6-4. Picoline ground state. (*Top*) 2D diffraction pattern. (*Bottom*) Refined ground-state structure of picoline. Comparison between the experimental and refined theoretical *f*(*r*) curves is shown.

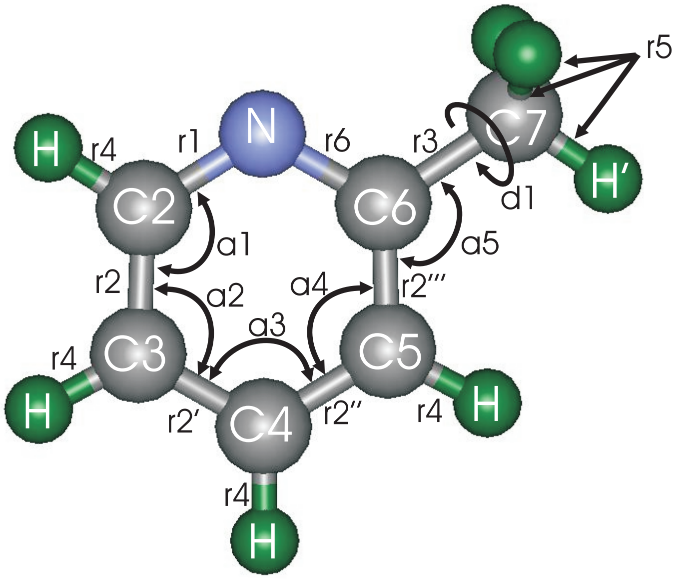

Distances

r1(N-C2)	1.328 ± 0.027	(1.334)
r2(C2-C3)	1.410 ± 0.004	(1.393)
r3(C6-C7)	1.525 ± 0.008	(1.507)
r4(C2-H)	1.096 ± 0.012	(1.083-1.087)
r5(C7-H')	1.185 ± 0.026	(1.091-1.093)
r2'(C3-C4)	1.402	(1.391)
r2"(C4-C5)	1.402	(1.391)
r2'"(C5-C6)	1.404	(1.393)
r6(N-C6)	1.374	(1.341)

Angles

a1(N-C2-C3)	121.2 ± 3.1	(123.8)
a2(C2-C3-C4)	118.4 ± 2.0	(117.9)
a3(C3-C4-C5)	119.7 ± 1.9	(118.8)
a4(C4-C5-C6)	117.4 ± 2.0	(119.3)
a5(C5-C6-C7)	119.5 ± 1.3	(121.8)
d1(C5C6C7H')	-176.6 ± 107.6	(121.2)

Figure 6-5. Refined ground-state structure of picoline. Distances are in ångströms and angles are in degrees. DFT values for the structural parameters are given in parentheses. The distances marked in blue were not independently refined, but derived from other best-fit (refined) distances in the structure.

2,6-Lutidine

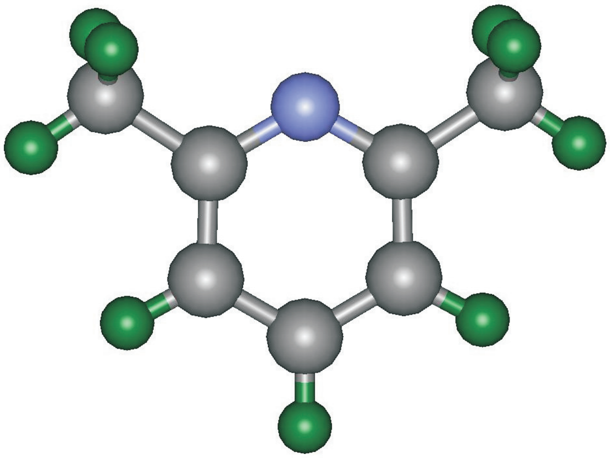

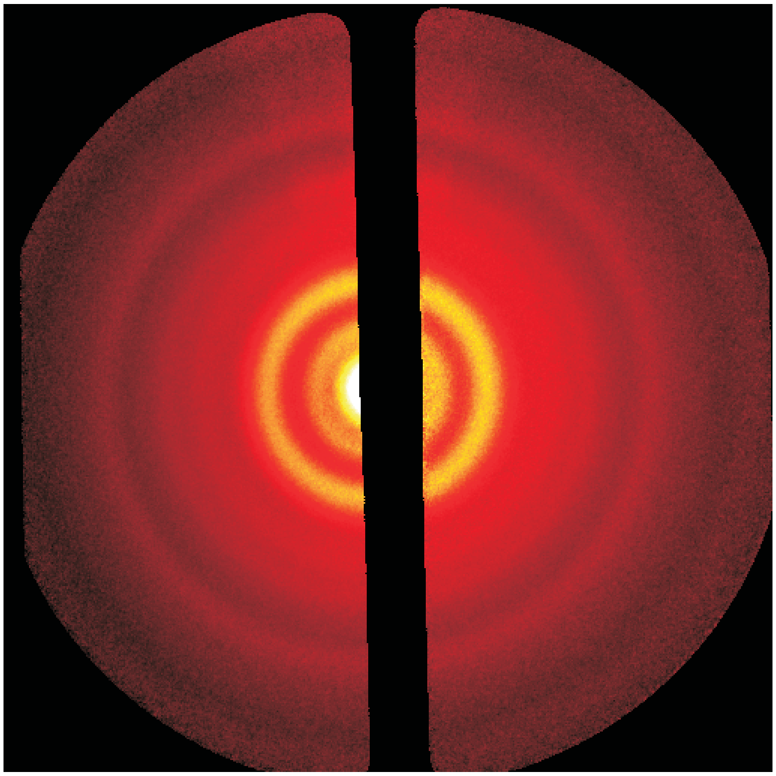

Figure 6-6. 2D ground state diffraction pattern of 2,6-lutidine.

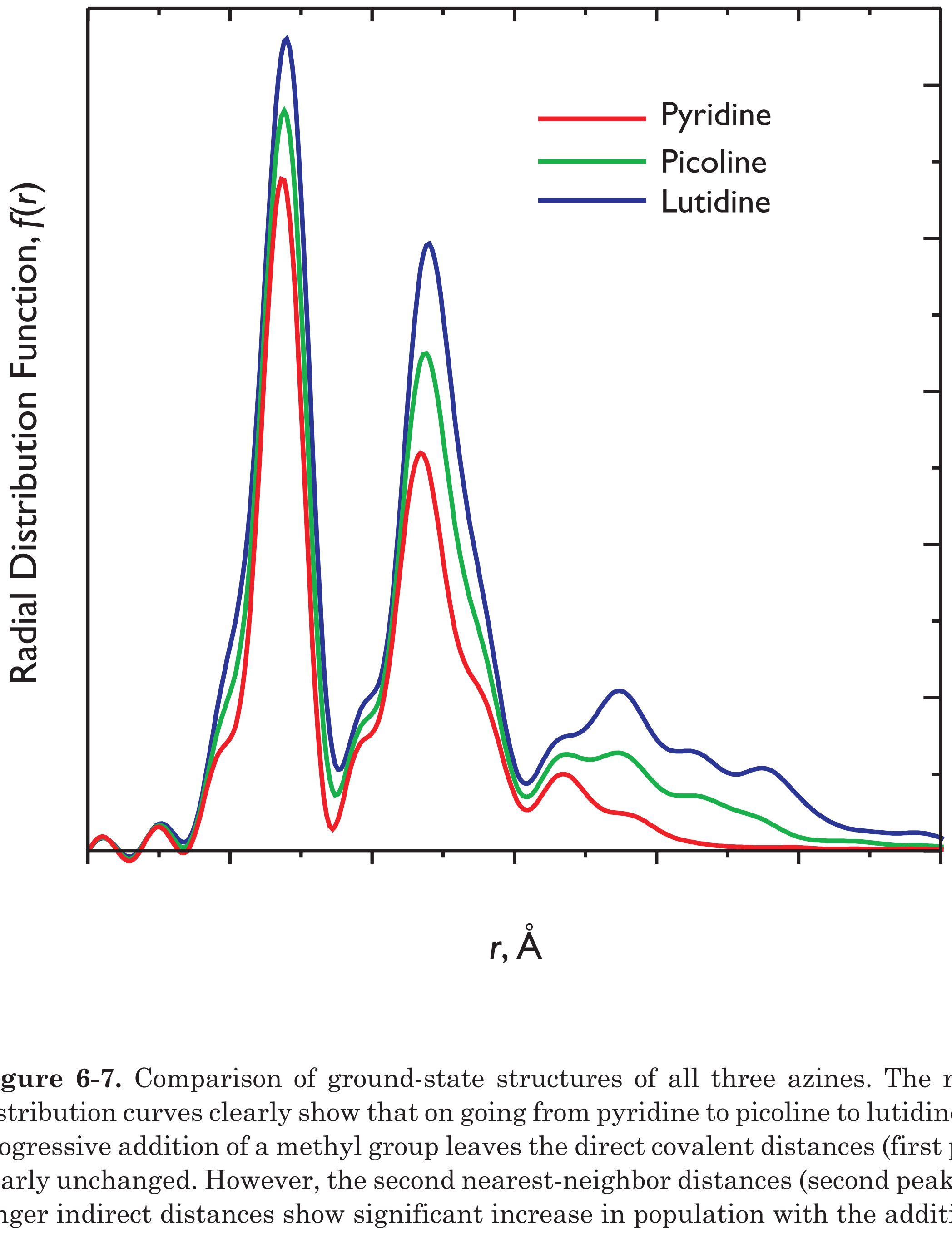

Figure 6-7. Comparison of ground-state structures of all three azines. The radial distribution curves clearly show that on going from pyridine to picoline to lutidine, the progressive addition of a methyl group leaves the direct covalent distances (first peak) nearly unchanged. However, the second nearest-neighbor distances (second peak) and longer indirect distances show significant increase in population with the addition of the methyl groups.

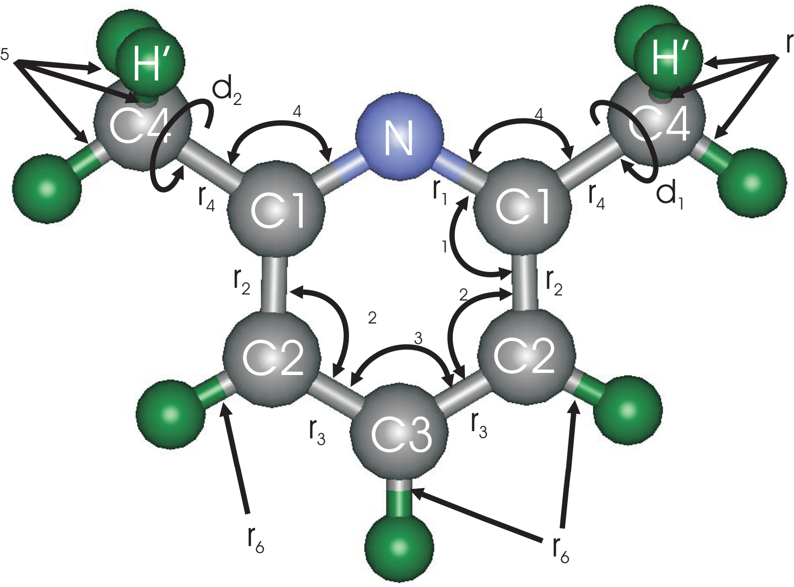

Distances

r_1(N-C1)	1.328 ± 0.059	(1.339)
r_2(C1-C2)	1.431 ± 0.008	(1.398)
r_3(C2-C3)	1.386 ± 0.007	(1.390)
r_4(C1-C4)	1.501 ± 0.005	(1.507)
r_5(H-C4)	1.090 ± 0.009	(1.092-1.093)
r_6(H-C2,H-C3)	1.101 ± 0.017	(1.084-1.085)

Angles

$_1$(N-C1-C2)	120.5 ± 1.1	(122.0)
$_2$(C1-C2-C3)	116.9 ± 0.5	(118.8)
$_3$(C2-C3-C2)	122.4 ± 1.0	(119.1)
$_4$(N-C1-C4)	118.4 ± 0.4	(116.2)
d_1(NC1C4H')	39.1 ± 4.0	(58.8)
d_2(NC1C4H')	1.1 ± 19.8	(58.8)

Figure 6-8. Refined ground-state structure of lutidine. Distances are in ångströms and angles are in degrees. DFT values for the structural parameters are given in parentheses.

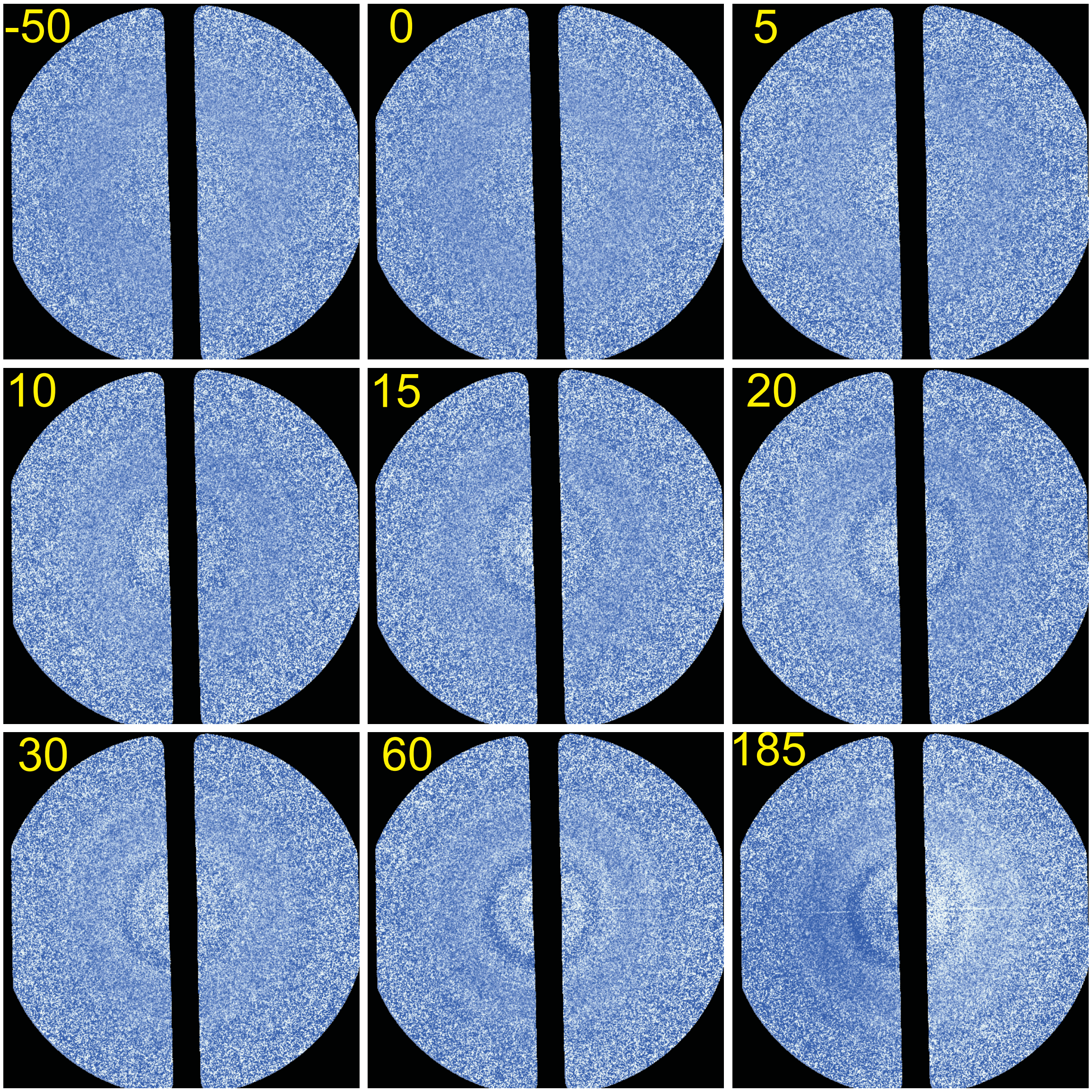

Figure 6-9. Time-resolved 2D diffraction-difference images of pyridine ($t_{\mathrm{ref}} = -90$ ps). Each frame is identified by the relative time delay (in picoseconds) between the laser pump and electron probe pulses. The emergence of rings in the difference images with increasing time delay reflects the ensuing molecular structural dynamics.

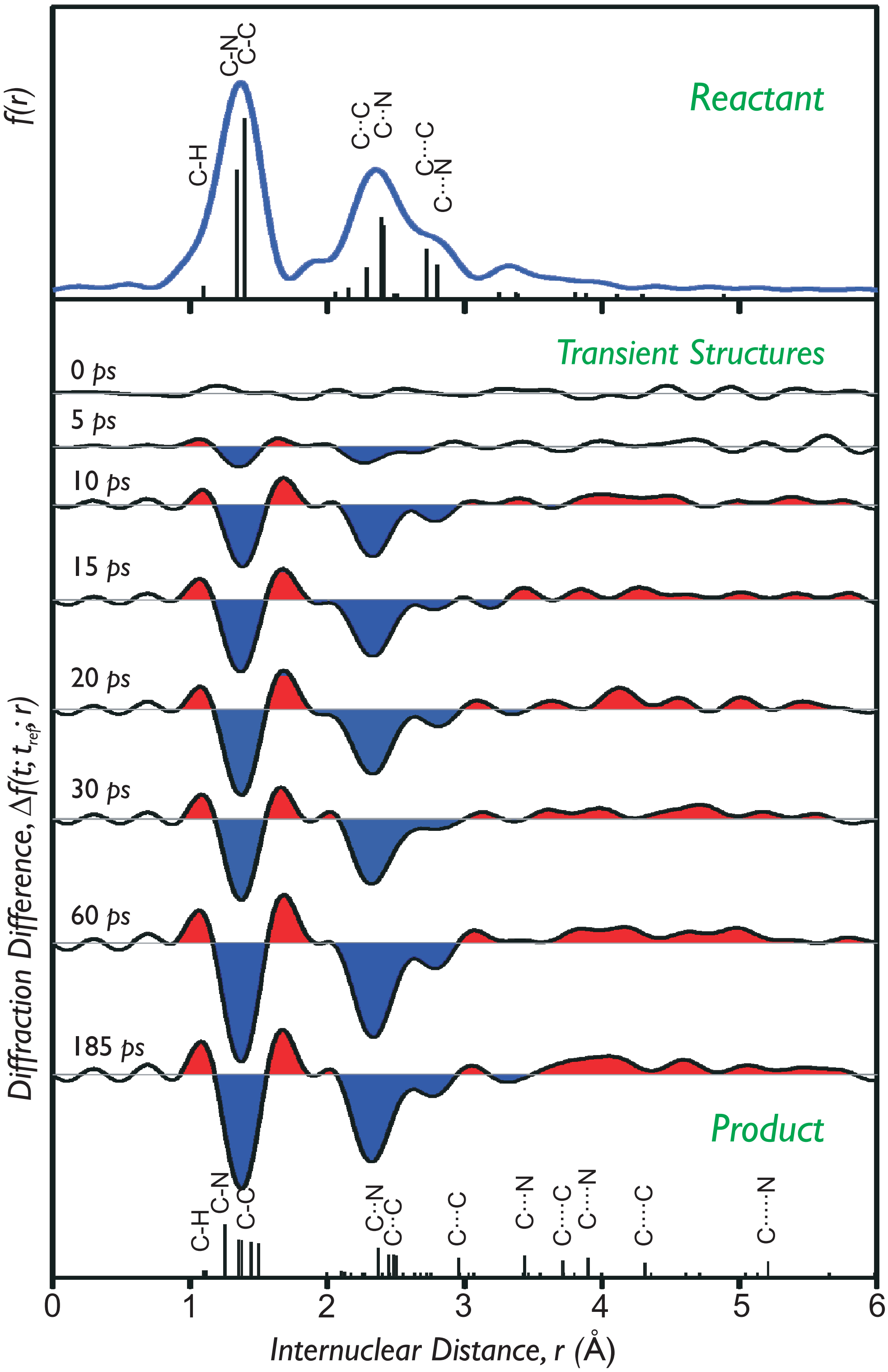

Figure 6-10. Radial distribution curves for pyridine. Parent (*top*) and $\Delta f(t, t_{\text{ref}}, r)$ curves (*bottom*). The vertical lines at the bottom indicate the relative contributions from various internuclear pairs, with the height of each line scaling with $(Z_iZ_j)/r_{ij}$ multiplied by the degeneracy. The *blue* highlighted regions represent net depletion of internuclear pairs (old bonds), whereas the *red* highlighted regions correspond to internuclear pairs with increasing population (new bonds).

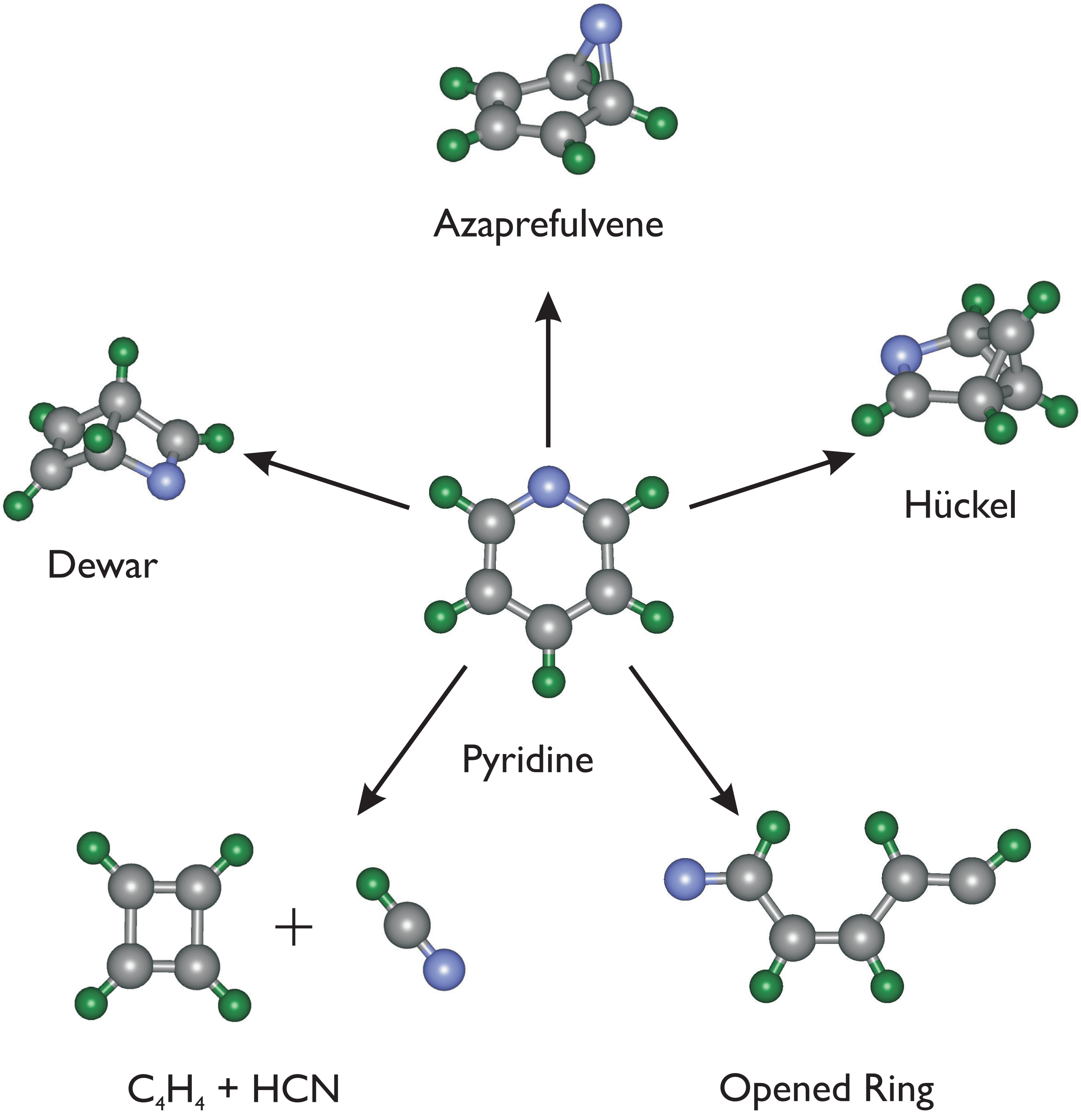

Figure 6-11. Possible structures from reaction of pyridine.

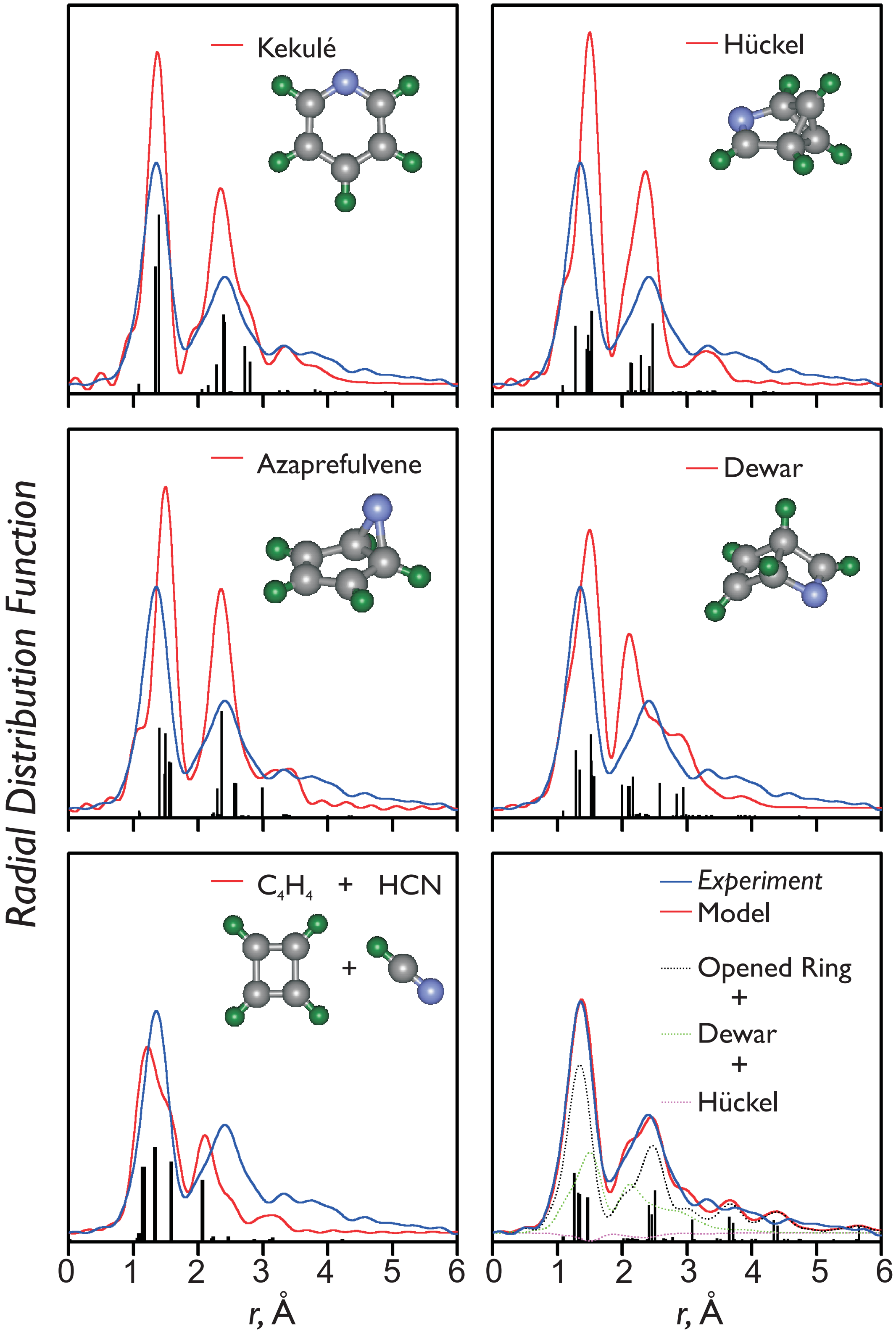

Figure 6-12. Comparisons of the experimental transient-isolated radial distribution $f(r)$ curve (blue) with normalized theoretical $f(r)$ curves (red), predicted for structures resulting from possible reaction channels. Discrepancies between theory and experiment are evident for all channels but one: that of the ring-opened structure with minor contributions from isomers.

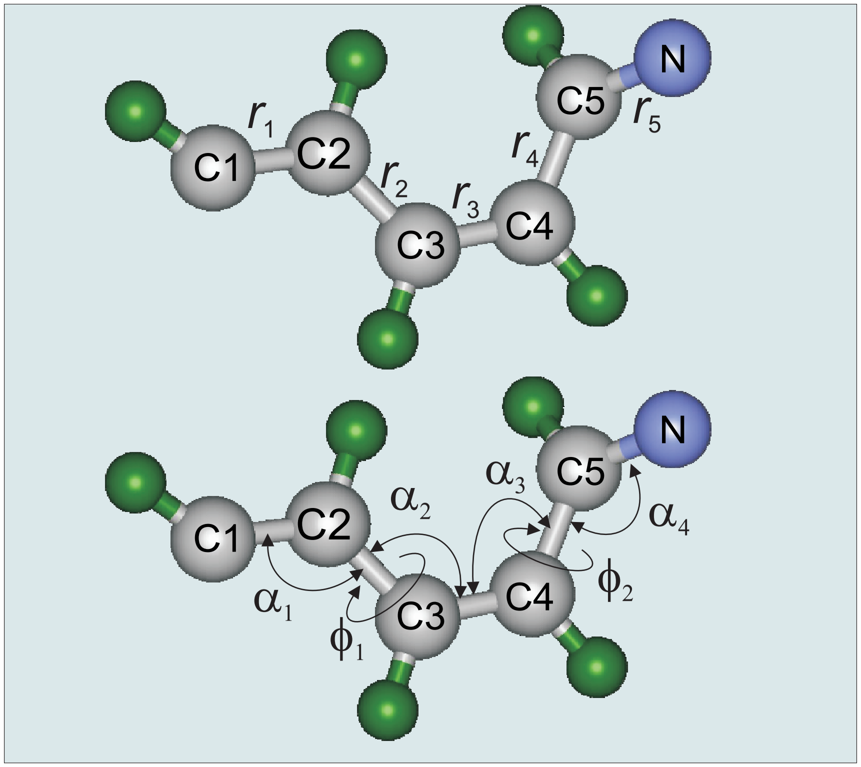

Distances

	experiment	*DFT*
r_1(C1-C2)	1.366 ± 0.011	1.318
r_2(C2-C3)	1.433 ± 0.012	1.456
r_3(C3-C4)	1.342 ± 0.033	1.348
r_4(C4-C5)	1.487 ± 0.018	1.466
r_5(C5-N)	1.244 ± 0.014	1.256

Angles

	experiment	*DFT*
α_1(C1-C2-C3)	127.7 ± 4.3	124.4
α_2(C2-C3-C4)	124.3 ± 3.3	127.0
α_3(C3-C4-C5)	123.4 ± 3.6	125.7
α_4(C4-C5-N)	121.1 ± 2.7	124.4
ϕ_1(C1C2-C3C4)	185 ± 36	180
ϕ_2(NC5-C4C3)	-123 ± 4	-180

Figure 6-13. Refined structural parameters for the pyridine ring-opened product compared to the corresponding values predicted by quantum chemical calculations. Distances are in ångströms, and angles are in degrees. Note that while the quantum calculations are for the *equilibrium* ring-opened structure, our refined structure accounts also for torsions that have a low-energy barrier; hence the discrepancy in ϕ_2.

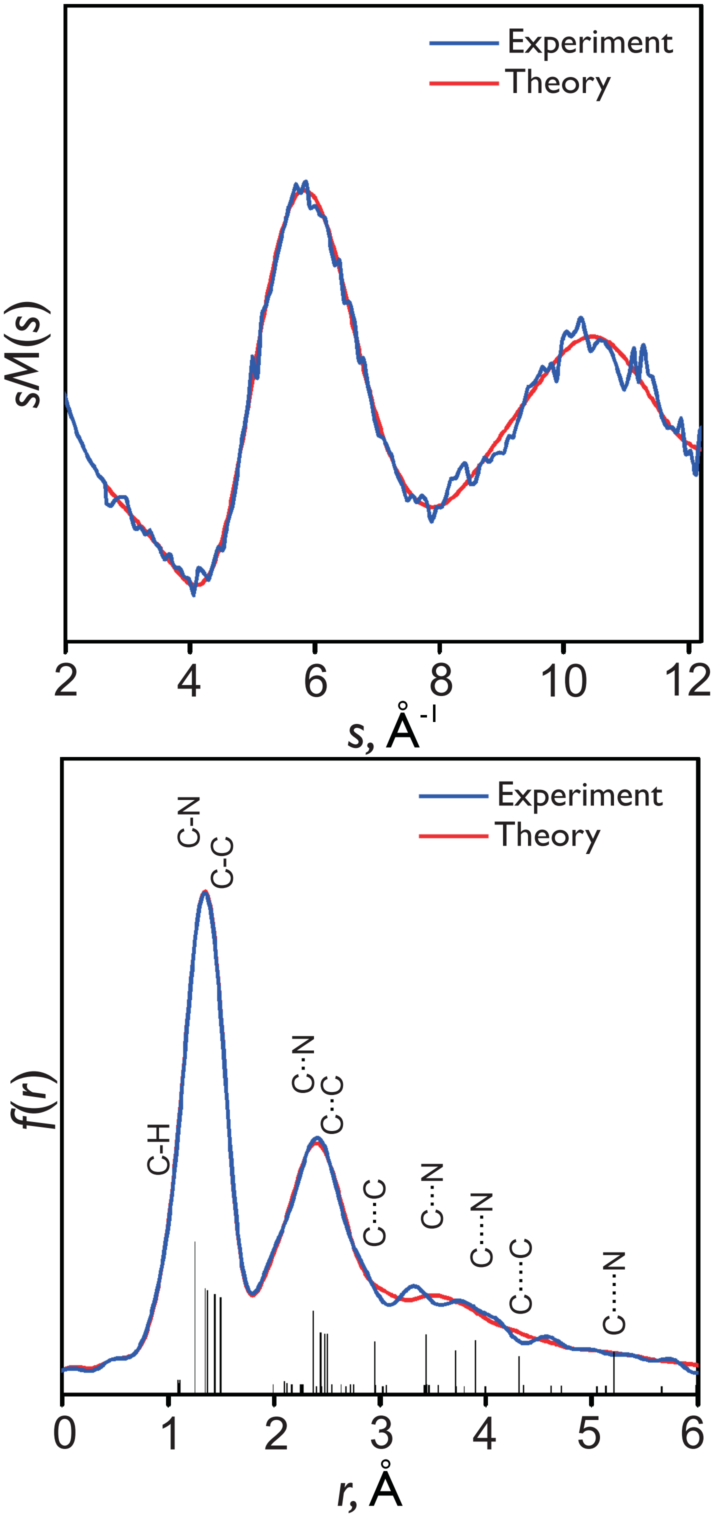

Figure 6-14. Refined ring-opened pyridine structure. Shown are the experimental diffraction (time-averaged) transient-only curves (blue) compared to theoretical curves corresponding to the ring-opened structure with mean *l* values 70-100% larger than those obtained at 403 K (red). The modified molecular scattering *sM*(*s*) curves are shown on top, and the corresponding radial distribution *f*(*r*) curves are shown below.

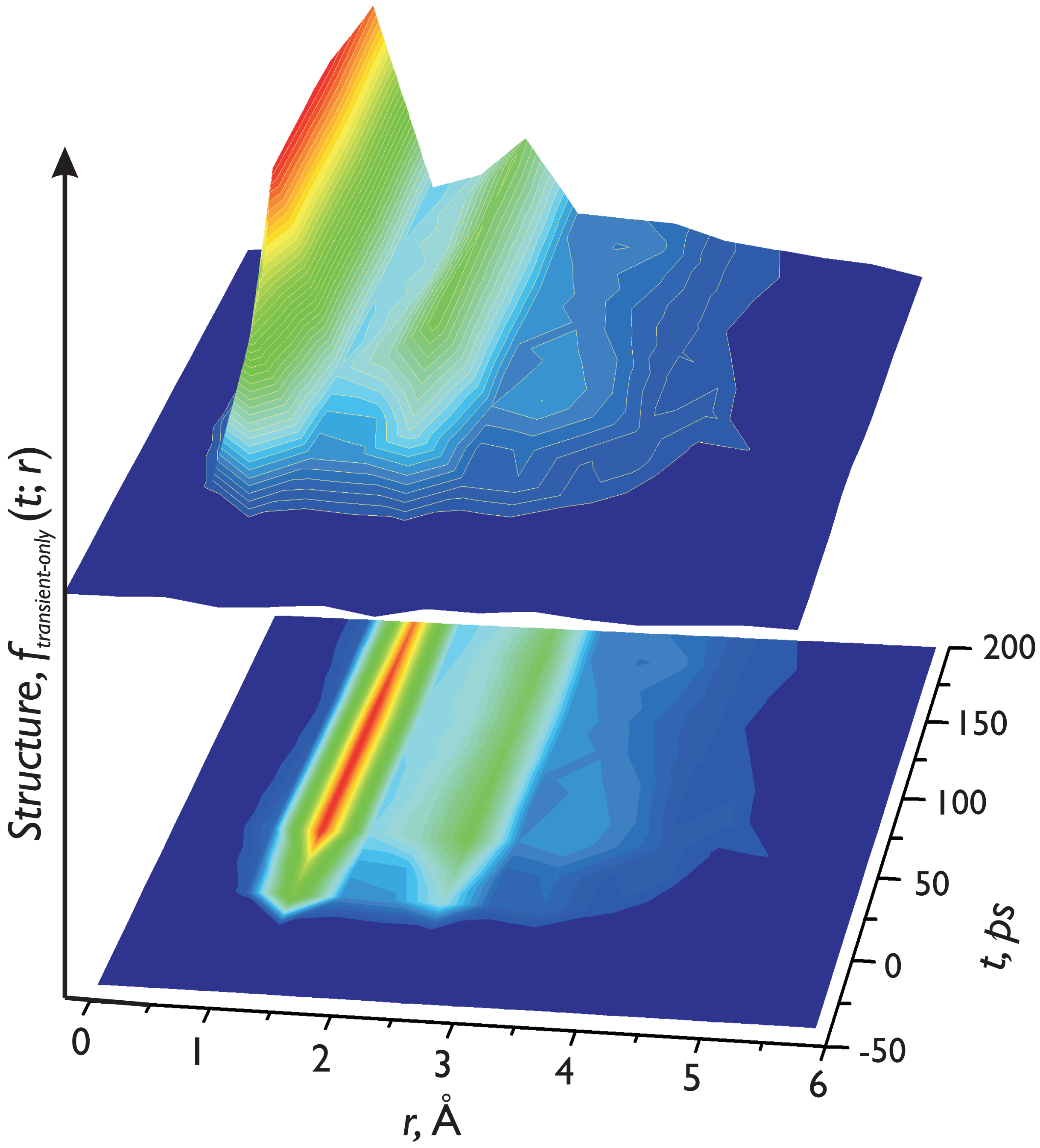

Figure 6-15. Pyridine structure and population change with time. The transient-isolated *f*(*r*) curves show the formation of product structures following excitation. The 2D plot indicates the range of internuclear distances (0-6 Å) and their change as a function of time; see text.

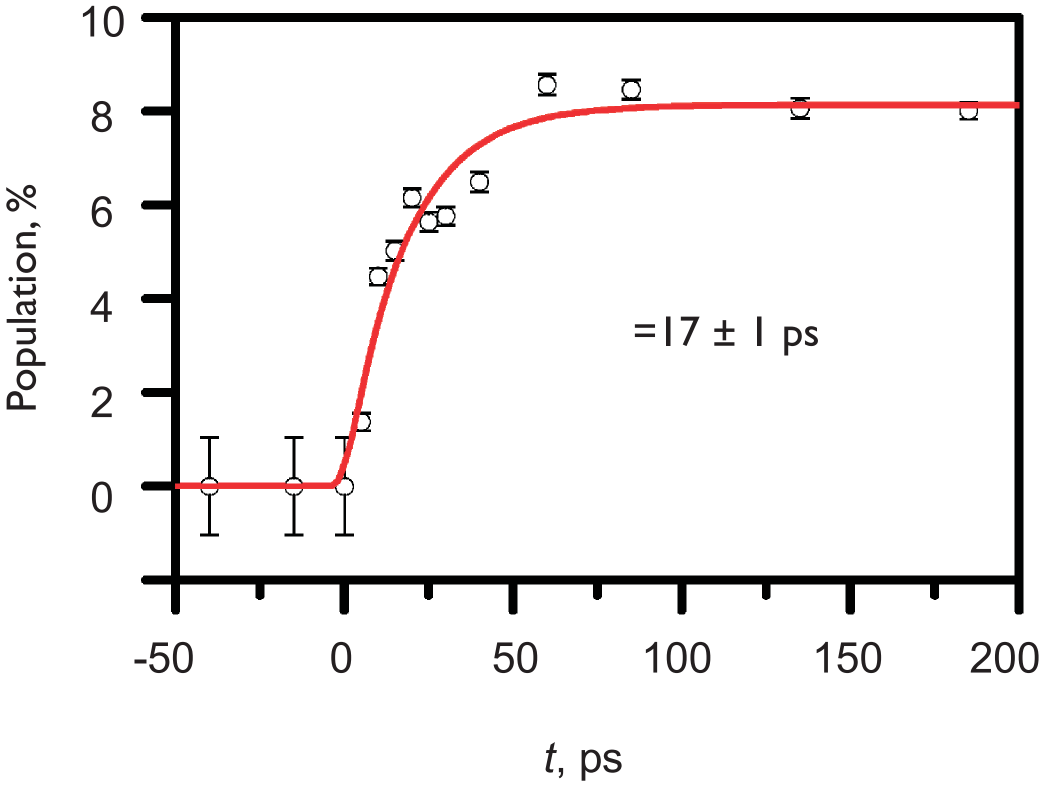

Figure 6-16. Temporal dependence of the product fraction, which fits a single-component rise (i.e., the formation of the pyridine ring-opened structure) and yields a time constant of 17 ± 1 ps.

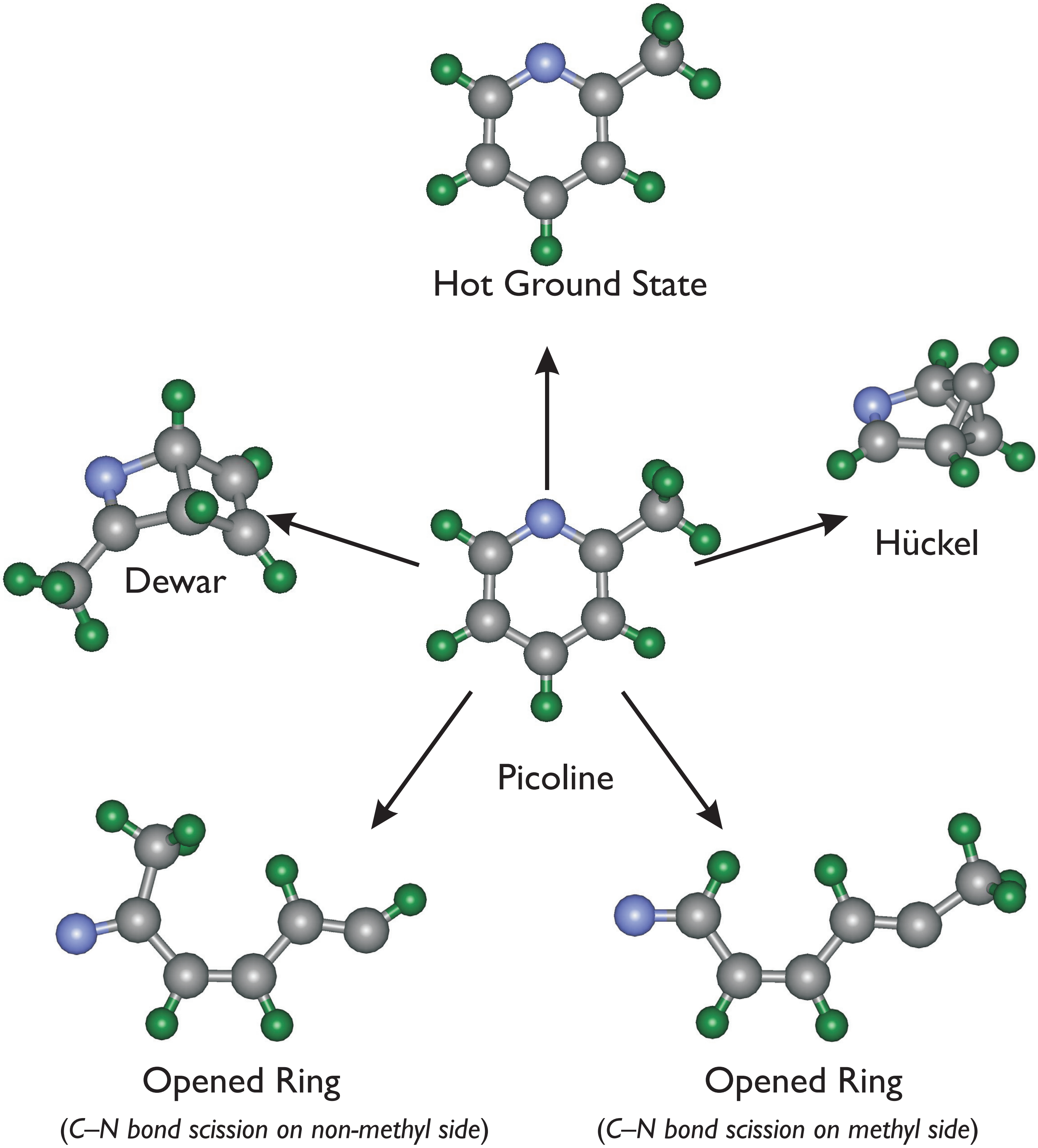

Figure 6-17. Possible structures from reaction of picoline.

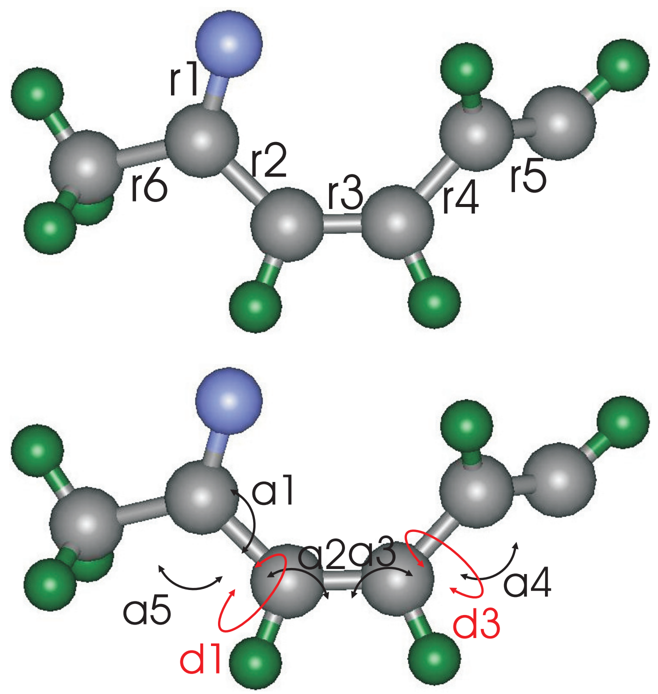

Distances

r1(N-C1)	1.277 ± 0.022	(1.259)
r2(C1-C2)	1.483 ± 0.009 *	(1.485)
r3(C2-C3)	1.346 ± 0.010 **	(1.345)
r4(C3-C4)	1.463 *	(1.454)
r5(C4-C5)	1.316 **	(1.313)
r6(C1-C6)	1.527 *	(1.525)

Angles

a1(N-C1-C2)	116.6 ± 2.4 *	(124.4)
a2(C1-C2-C3)	134.3 ± 2.0 **	(125.9)
a3(C2-C3-C4)	133.3 **	(124.3)
a4(C3-C4-C5)	128.6 ± 11.9	(126.4)
a5(C6-C1-C2)	121.7 *	(116.5)
d1(N-C1,C2-C3)	-21.7 ± 34.7	(0.0)
d2(C2-C3,C4-C5)	-127.3 ± 33.2	(180.0)

Figure 6-18. Refined structural parameters for the picoline ring-opened product compared to the corresponding values predicted by quantum chemical calculations (given in parentheses). Distances are in ångströms, and angles are in degrees. Note that while the quantum calculations are for the *equilibrium* ring-opened structure, our refined structure accounts also for torsions that have a low-energy barrier. The parameters marked with * and ** were not independently refined, but were derived from other best-fit distances.

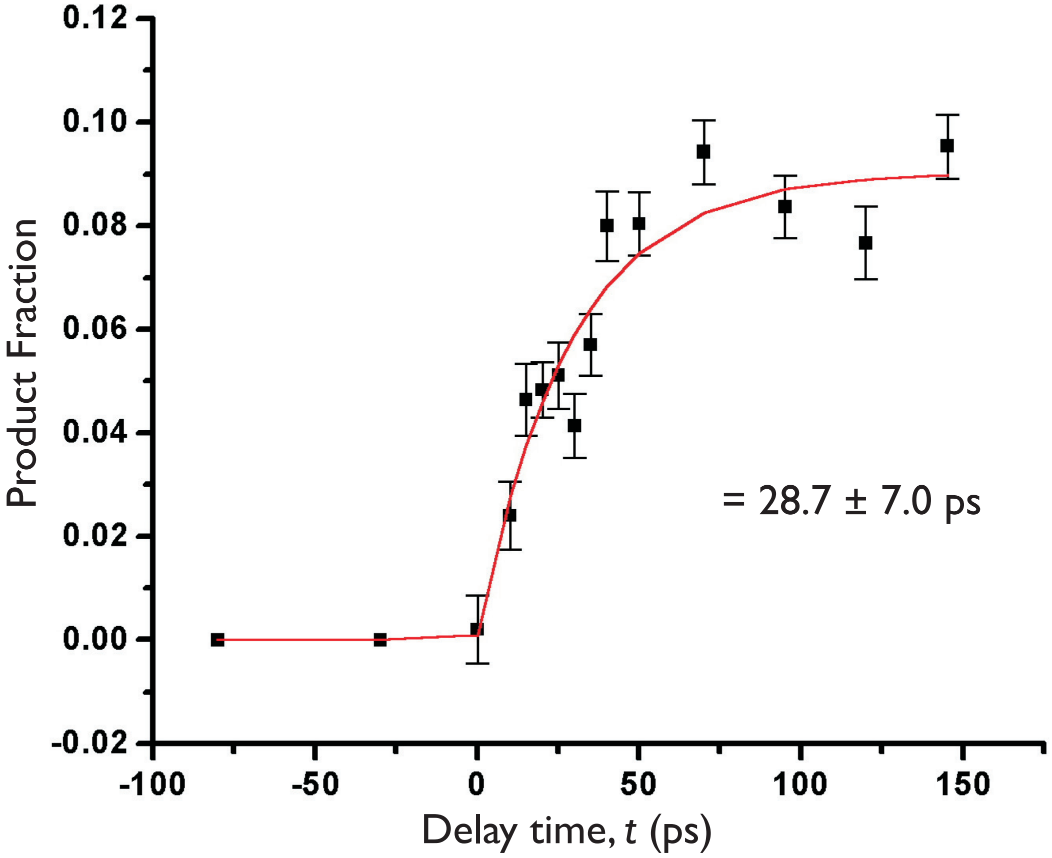

Figure 6-19. Temporal dependence of the product fraction, which fits a single-component rise (i.e., the formation of the picoline ring-opened structure) and yields a time constant of 28.7 ± 7.0 ps.

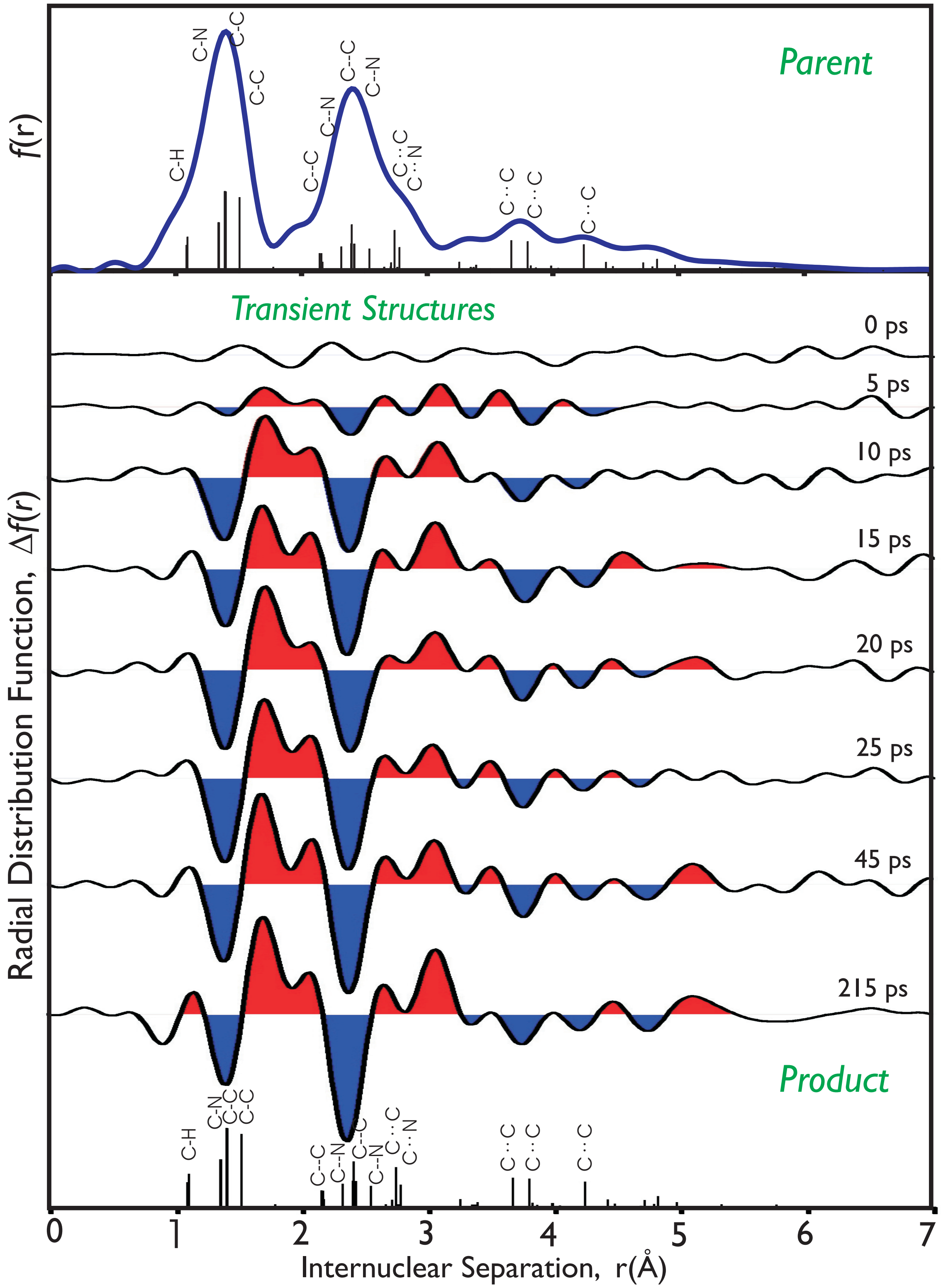

Figure 6-20. Radial distribution curves for lutidine. Parent (*top*) and $\Delta f(t, t_{\text{ref}}, r)$ curves (*bottom*). The *blue* highlighted regions represent net depletion of internuclear pairs, whereas the *red* highlighted regions correspond to internuclear pairs with increasing population.

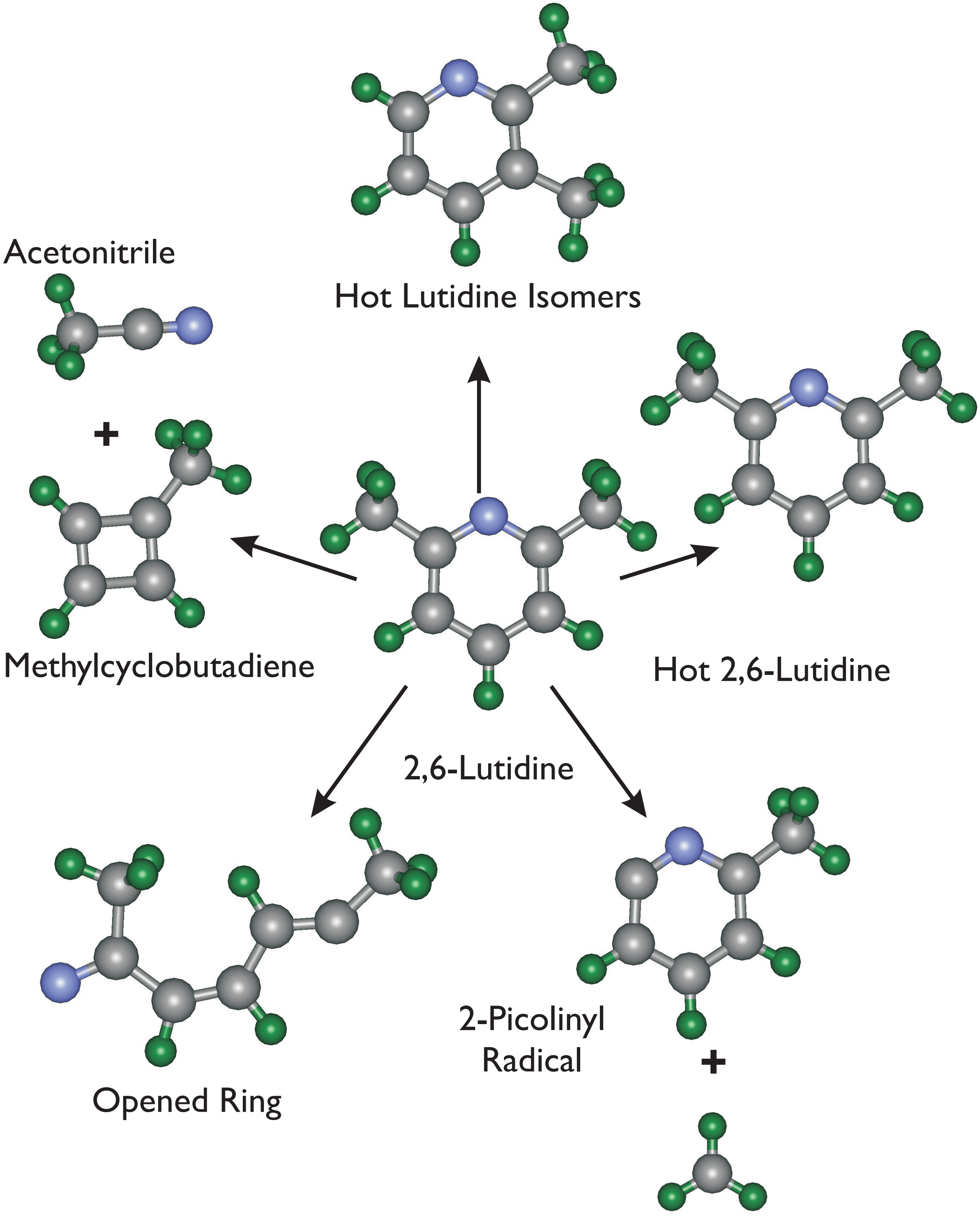

Figure 6-21. Possible structures from reaction of lutidine.

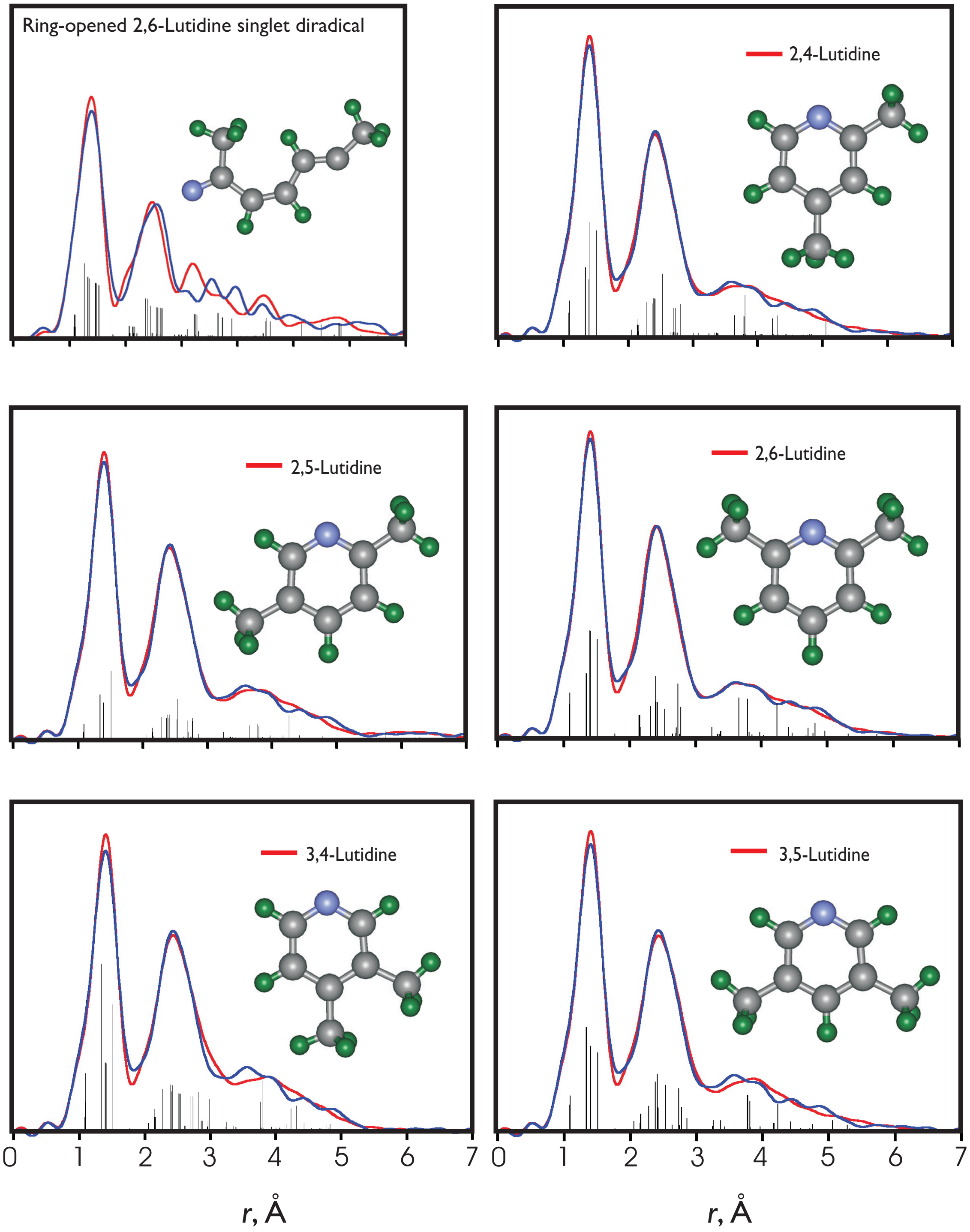

Figure 6-22. Comparisons of the experimental transient-isolated radial distribution *f*(*r*) curve (blue) to normalized theoretical *f*(*r*) curves (red), predicted for the structures resulting from various possible reaction channels. Unlike pyridine, the ring-opened diradical structure does not fit the data. However, the hot ground-state of lutidine isomers provides excellent fit to the data.

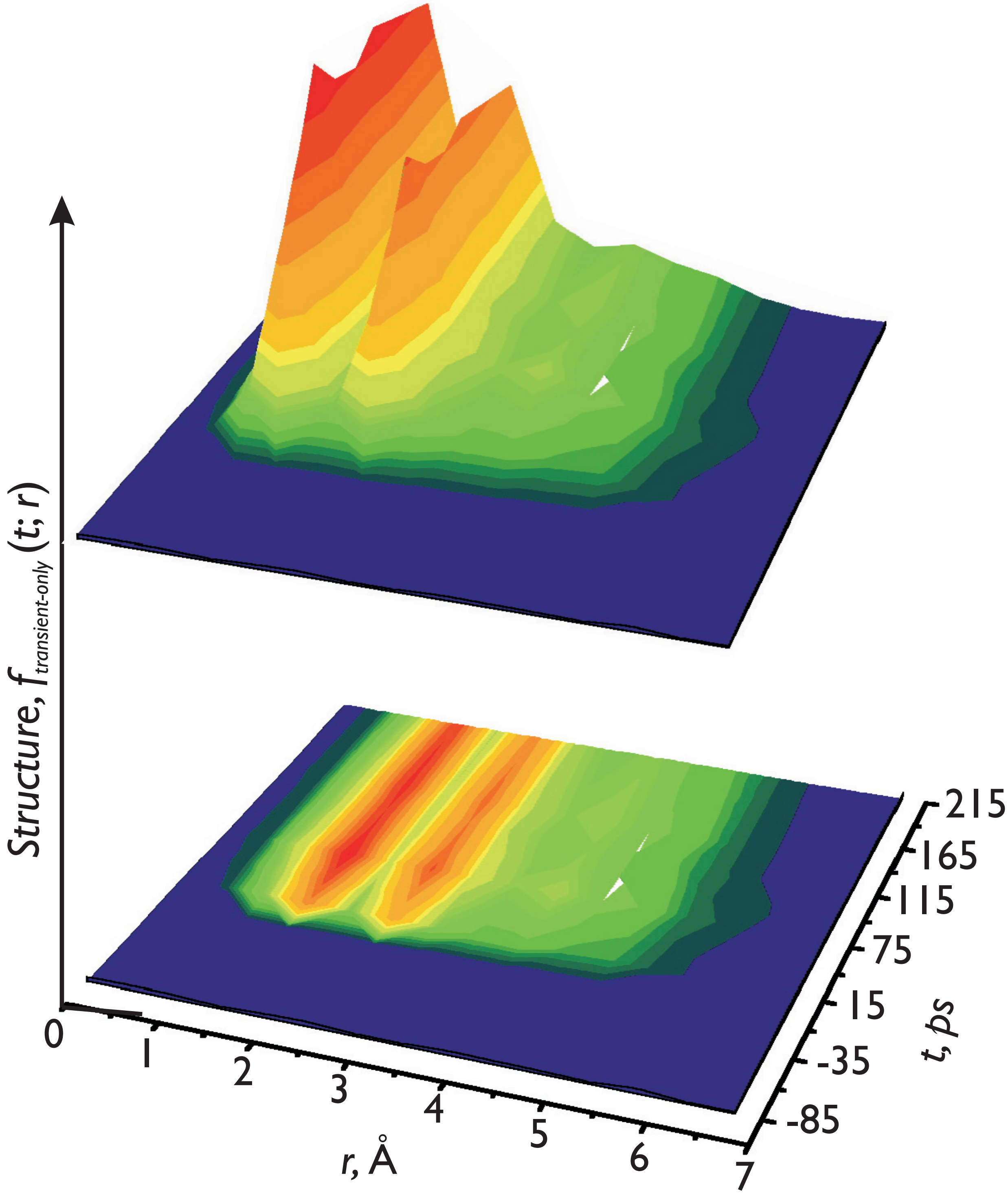

Figure 6-23. Lutidine structure and population change with time. The transient-isolated $f(r)$ curves show the formation of product structures following excitation. The 2D plot indicates the range of internuclear distances (0-7 Å) and their change as a function of time; see text.

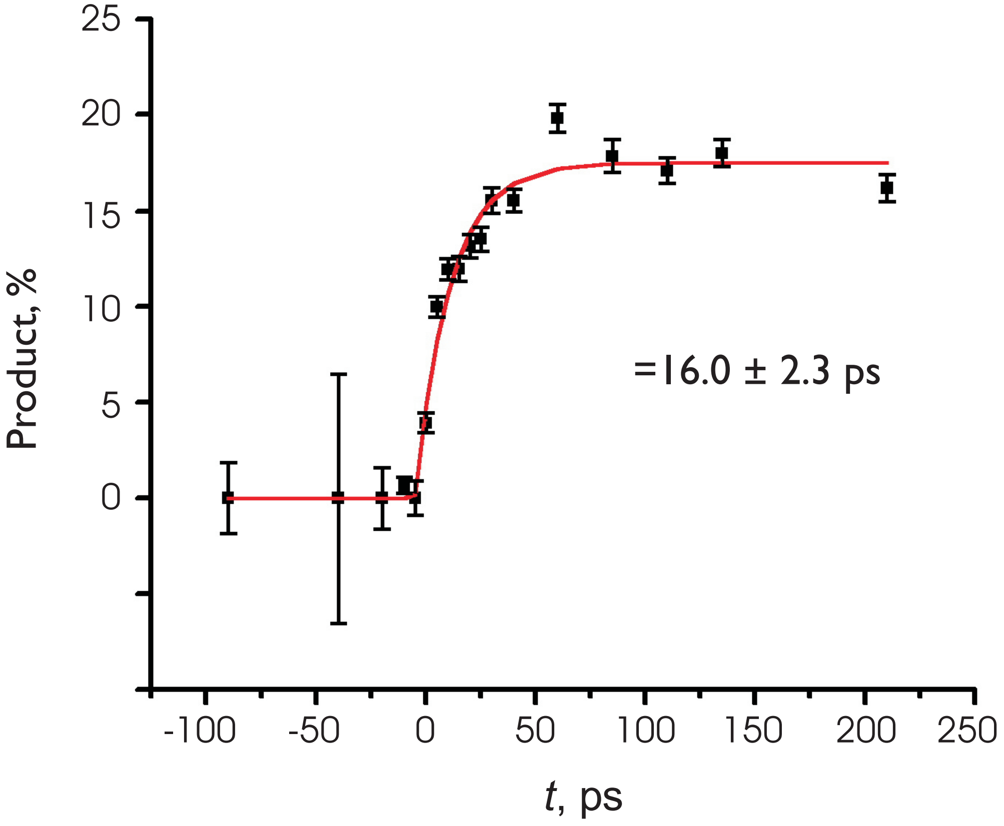

Figure 6-24. Temporal dependence of the product fraction, which fits a single-component rise (i.e., the formation of the lutidine hot ground-state structures) and yields a time constant of 16 ± 2.3 ps.

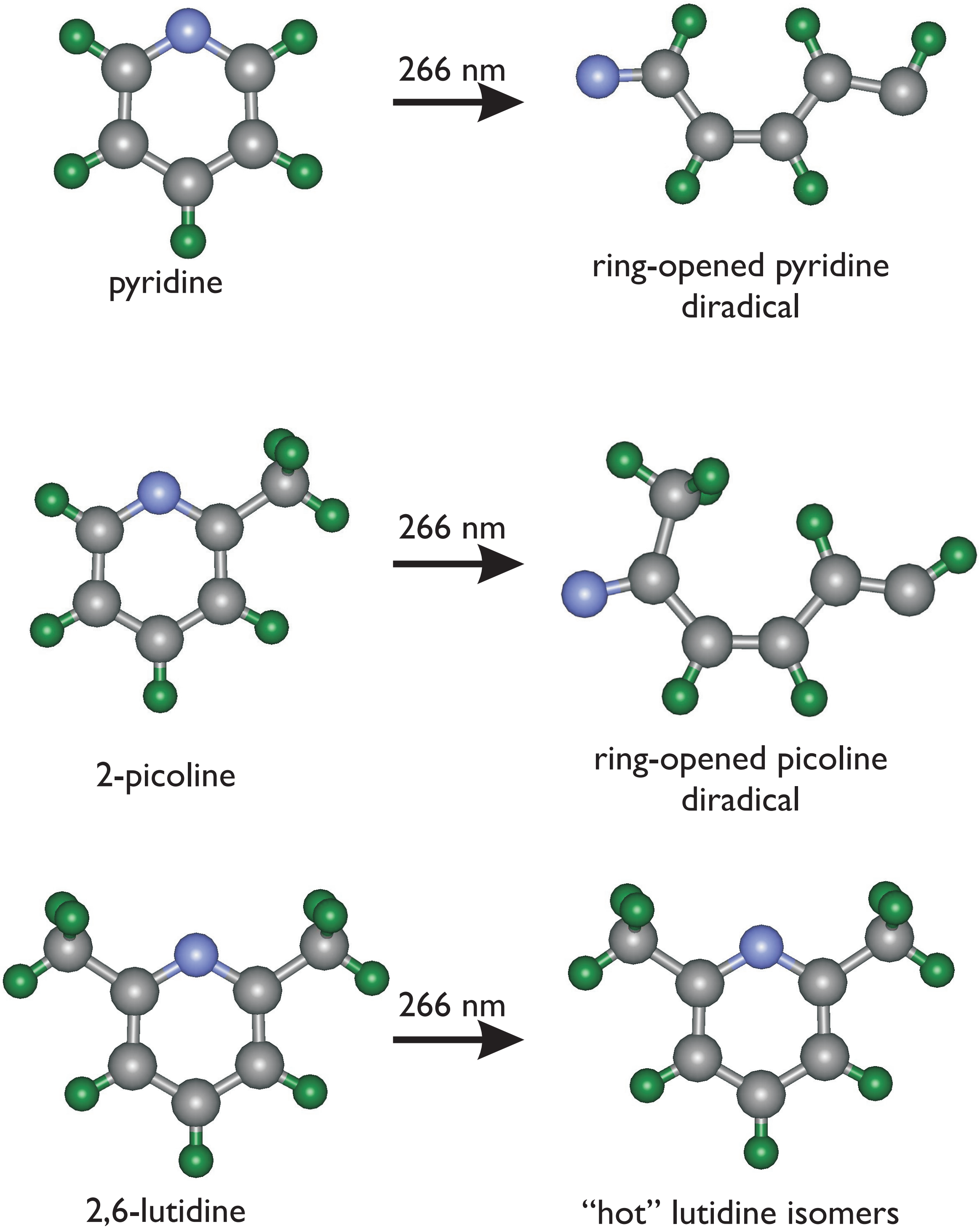

Figure 6-25. Photochemistry of azines elucidated by UED-3.

References

1. Otis, C. E.; Knee, J. L.; Johnson, P. M., *J. Phys. Chem.* **1983,** *87*, 2232.
2. Villa, E.; Amirav, A.; Lim, E. C., *J. Phys. Chem.* **1988,** *92*, 5393.
3. Callomon, J. H.; Parkin, J. E.; Lopezdel. R, *Chem. Phys. Lett.* **1972,** *13*, 125.
4. Knight, A. E. W.; Parmenter, C. S., *Chem. Phys.* **1976,** *15*, 85.
5. Yamazaki, I.; Baba, H., *J. Chem. Phys.* **1977,** *66*, 5826.
6. Yamazaki, I.; Sushida, K.; Baba, H., *J. Chem. Phys.* **1979,** *71*, 381.
7. Hochstrasser, R. M.; Marzzacco, C. A., In *Molecular Luminescence*, Lim, E. C., Ed., Benjamin: New York, 1969.
8. Wassam, W. A.; Lim, E. C., *J. Chem. Phys.* **1978,** *68*, 433.
9. Wassam, W. A.; Lim, E. C., *Chem. Phys. Lett.* **1977,** *52*, 295.
10. Wassam, W. A.; Lim, E. C., *J. Chem. Phys.* **1978,** *69*, 2175.
11. Wassam, W. A.; Lim, E. C., *J. Mol. Struct.* **1978,** *47*, 129.
12. Lim, E. C., *J. Phys. Chem.* **1986,** *90*, 6770.
13. Yamazaki, I.; Murao, T.; Yamanaka, T.; Yoshihara, K., *Faraday Discuss.* **1983**, 395.
14. Yamazaki, I.; Murao, T.; Yoshihara, K.; Fujita, M.; Sushida, K.; Baba, H., *Chem. Phys. Lett.* **1982,** *92*, 421.
15. Yamazaki, I.; Sushida, K.; Baba, H., *J. Lumines.* **1979,** *18-9*, 425.

16. Ihee, H.; Lobastov, V. A.; Gomez, U.; Goodson, B. M.; Srinivasan, R.; Ruan, C.-Y.; Zewail, A. H., *Science* **2001,** *291*, 458.

17. Srinivasan, R.; Lobastov, V. A.; Ruan, C. Y.; Zewail, A. H., *Helv. Chim. Acta* **2003,** *86*, 1763.

18. Vigliotti, F.; Chen, S. Y.; Ruan, C. Y.; Lobastov, V. A.; Zewail, A. H., *Angew. Chem.-Int. Edit.* **2004,** *43*, 2705.

19. Ruan, C. Y.; Lobastov, V. A.; Vigliotti, F.; Chen, S. Y.; Zewail, A. H., *Science* **2004,** *304*, 80.

20. Ruan, C. Y.; Vigliotti, F.; Lobastov, V. A.; Chen, S. Y.; Zewail, A. H., *Proc. Natl. Acad. Sci. USA* **2004,** *101*, 1123.

21. Thomas, J. M., *Angew. Chem.-Int. Edit.* **2004,** *43*, 2606.

22. Schomaker, V.; Pauling, L., *J. Am. Chem. Soc.* **1939,** *61*, 1769.

23. Almenningen, A.; Bastiansen, O.; Hansen, L., *Acta Chem. Scand.* **1955,** *9*, 1306.

24. Pyckhout, W.; Horemans, N.; Van Alsenoy, C.; Geise, H. J.; Rankin, D. W. H., *J. Mol. Struct.* **1987,** *156*, 315.

25. Mootz, D.; Wussow, H.-G., *J. Chem. Phys.* **1981,** *75*, 1517.

26. Mata, F.; Quintana, M. J.; Sørensen, G. O., *J. Mol. Struct.* **1977,** *42*, 1.

27. Wong, K. N.; Colson, S. D., *J. Mol. Spectrosc.* **1984,** *104*, 129.

28. Walters, V. A.; Snavely, D. L.; Colson, S. D.; Wiberg, K. B.; Wong, K. N., *J. Phys. Chem.* **1986,** *90*, 592.

29. Ureña, F. P.; Gómez, M. F.; González, J. J. L.; Torres, E. M., *Spectroc. Acta Pt. A-Molec. Biomolec. Spectr.* **2003,** *59*, 2815.

30. Kjaergaard, H. G.; Proos, R. J.; Turnbull, D. M.; Henry, B. R., *J. Phys. Chem.* **1996,** *100*, 19273.

31. Cai, Z.-L.; Reimers, J. R., *J. Phys. Chem. A* **2000,** *104*, 8389.

32. Fabian, J.; Lewars, E., *Can. J. Chem.-Rev. Can. Chim.* **2004,** *82*, 50.

33. Martin, J. M. L.; VanAlsenoy, C., *J. Phys. Chem.* **1996,** *100*, 6973.

34. Szafran, M.; Koput, J., *J. Mol. Struct.* **2001,** *565*, 439.

35. Becucci, M.; Lakin, N. M.; Pietraperzia, G.; Salvi, P. R.; Castellucci, E.; Kerstel, E. R. T., *J. Chem. Phys.* **1997,** *107*, 10399.

36. Bond, A. D.; Davies, J. E., *Acta Crystallogr. Sect. E.-Struct Rep. Online* **2001,** *57*, 01089.

37. Vorontsov, I. I.; Almásy, L.; Antipin, M. Y., *J. Mol. Struct.* **2002,** *610*, 271.

38. Bond, A. D.; Davies, J. E.; Kirby, A. J., *Acta Crystallogr. Sect. E.-Struct Rep. Online* **2001,** *57*, O1242.

39. Porcinai, S.; Foggi, P., *Nuovo Cimento Soc. Ital. Fis. D-Condens. Matter At. Mol. Chem. Phys. Fluids Plasmas Biophys.* **1997,** *19*, 889.

40. Zhong, D. P.; Diau, E. W. G.; Bernhardt, T. M.; De Feyter, S.; Roberts, J. D.; Zewail, A. H., *Chem. Phys. Lett.* **1998,** *298*, 129.

41. Prather, K. A.; Lee, Y. T., *Isr. J. Chem.* **1994,** *34*, 43.

42. Wilzbach, K. E.; Rausch, D. J., *J. Am. Chem. Soc.* **1970,** *92*, 2178.

43. Chachisvilis, M.; Zewail, A. H., *J. Phys. Chem. A* **1999,** *103*, 7408.

44. Chapman, O. L.; McIntosh, C. L.; Pacansky, J., *J. Am. Chem. Soc.* **1973,** *95*, 614.

45. Johnstone, D. E.; Sodeau, J. R., *J. Phys. Chem.* **1991,** *95*, 165.

46. Kudoh, S.; Takayanagi, M.; Nakata, M., *J. Photochem. Photobiol. A-Chem.* **1999,** *123*, 25.

47. Sobolewski, A. L.; Domcke, W., *Chem. Phys. Lett.* **1991,** *180*, 381.

48. Ruan, C. Y.; Lobastov, V. A.; Srinivasan, R.; Goodson, B. M.; Ihee, H.; Zewail, A. H., *Proc. Natl. Acad. Sci. USA* **2001,** *98*, 7117.

49. Caplain, S.; Catteau, J. P.; Lablache-Combier, A., *Journal of the Chemical Society D-Chemical Communications* **1970**, 1475.

50. Nakata, M., *Bull. Chem. Soc. Jpn.* **2002,** *75*, 1173.

51. Noyes, J., W. A.; Al-Ani, K. E., *Chem. Rev.* **1974,** *74*, 29.

52. Lemaire, J., *J. Phys. Chem.* **1967,** *71*, 612.

53. Linnell, R. H.; Noyes, W. A., *J. Am. Chem. Soc.* **1951,** *73*, 3986.

54. Mathias, E.; Heicklen, J., *Mol. Photochem.* **1972,** *4*, 483.

55. Chesko, J. D.; Lee, Y. T., In *Highly Excited Molecules*, 1997, 107.

56. Pavlik, J. W.; Laohhasurayotin, S., *Tetrahedron Lett.* **2003,** *44*, 8109.

57. Mackie, J. C.; Colket III, M. B.; Nelson, P. F., *J. Phys. Chem.* **1990,** *94*, 4099.

58. Jones, J.; Bacskay, G. B.; Mackie, J. C.; Doughty, A., *J. Chem. Soc.-Faraday Trans.* **1995,** *91*, 1587.

59. Politzer, P.; Murray, J. S.; Concha, M. C., *J. Phys. Chem. A* **1998,** *102*, 6697.

60. Barckholtz, C.; Barckholtz, T. A.; Hadad, C. M., *J. Am. Chem. Soc.* **1999,** *121*, 491.

61. Liu, R.; Huang, T. T.-S.; Tittle, J.; Xia, D., *J. Phys. Chem. A* **2000,** *104*, 8368.

62. Davico, G. E.; Bierbaum, V. M.; DePuy, C. H.; Ellison, G. B.; Squires, R. R., *J. Am. Chem. Soc.* **1995,** *117*, 2590.

63. Hore, N. R.; Russell, D. K., *J. Chem. Soc.-Perkin Trans. 2* **1998**, 269.

64. Kiefer, J. H.; Zhang, Q.; Kern, R. D.; Yao, J.; Jursic, B., *J. Phys. Chem. A* **1997,** *101*, 7061.

65. Yokoyama, A.; Zhao, X.; Hintsa, E. J.; Continetti, R. E.; Lee, Y. T., *J. Chem. Phys.* **1990,** *92*, 4222.

66. Sevy, E. T.; Muyskens, M. A.; Rubin, S. M.; Flynn, G. W.; Muckerman, J. T., *J. Chem. Phys.* **2000,** *112*, 5829.

67. Salcedo, R., *Theochem-J. Mol. Struct.* **2004,** *674*, 125.

68. Baldridge, K. K.; Gordon, M. S., *J. Am. Chem. Soc.* **1988,** *110*, 4204.

69. Caplain, S.; Lablanch.A, *Journal of the Chemical Society D-Chemical Communications* **1970**, 1247.

70. Roebke, W., *J. Phys. Chem.* **1970,** *74*, 4198.

71. Kudoh, S.; Takayanagi, M.; Nakata, M., *Chem. Phys. Lett.* **1999,** *308*, 403.

72. Egorova, M.; Zhao, Y.; Kukula, P.; Prins, R., *J. Catal.* **2002,** *206*, 263.

73. Doughty, A.; Mackie, J. C., *J. Phys. Chem.* **1992,** *96*, 10339.

74. Pavlik, J. W.; Kebede, N.; Thompson, M.; Day, A. C.; Barltrop, J. A., *J. Am. Chem. Soc.* **1999,** *121*, 5666.

75. Tsubouchi, M.; Suzuki, T., *J. Phys. Chem. A* **2003,** *107*, 10897.